

1-1-2017

Monte-Carlo-Simulation-Based, Product-Quality-Focused Analysis Of Nanocoating Curing And Post Curing Process

Jianming Zhao
Wayne State University,

Follow this and additional works at: https://digitalcommons.wayne.edu/oa_theses

 Part of the [Chemical Engineering Commons](#)

Recommended Citation

Zhao, Jianming, "Monte-Carlo-Simulation-Based, Product-Quality-Focused Analysis Of Nanocoating Curing And Post Curing Process" (2017). *Wayne State University Theses*. 600.
https://digitalcommons.wayne.edu/oa_theses/600

This Open Access Thesis is brought to you for free and open access by DigitalCommons@WayneState. It has been accepted for inclusion in Wayne State University Theses by an authorized administrator of DigitalCommons@WayneState.

**MONTE-CARLO-SIMULATION-BASED,
PRODUCT-QUALITY-FOCUSED ANALYSIS OF
NANOCOATING CURING AND POST CURING PROCESS**

By

JIANMING ZHAO

THESIS

Submitted to the Graduate School
Of Wayne State University,
Detroit, Michigan

In partial fulfillment of the requirements

For the degree of

MASTER OF SCIENCE

2017

MAJOR: CHEMICAL ENGINEERING

Approved by:

Advisor Date

ACKNOWLEDGMENTS

I want to express my sincere gratefulness to my advisor, Prof. Yinlun Huang, for his remarkable guidance, constant supervision, encouragement and moral support in the work of this thesis. Special thanks to Dr. Charles Manke and Dr. Steve Salley, for their valuable advice and suggestions to this thesis and for serving as members of the committee.

I also want to express my appreciation to Dr. Hao Song for his precious time to discuss with me about the research and constructive suggestions and providing me help both in academic and daily life.

I would like to thank Aida Amini-Rankouhi and other members of my group for their support and help.

Otherwise, I want to thank my family and my girlfriend for their patience, understanding, love and many sacrifices.

Table of Contents

ACKOWLEFGMENTS	ii
CHAPTER 1 INTRODUCTION	1
1.1 Nanoparticle Applied Polymer Coatings	1
1.2 Polymer Coating Curing and Post-curing Process	3
1.3 Process Modeling and Simulation.....	4
1.4 Thesis Overview and Contributions	5
CHAPTER 2 VALID PARAMETERS OF NANOCOATING	6
2.1 Effect of Nanoparticle Category.....	6
2.2 Effect of Nanoparticle Shape.....	11
2.3 Effect of Nanoparticle Heterogeneity.....	14
2.4 Challenges.....	17
2.5 Overview.....	19
CHAPTER 3 COMPUTATIONAL SIMULATION METHODOLOGY	21
3.1 Off-Lattice Simulation	22
3.2 Kinetics Simulation	24
3.3 Potential Energy Models.....	28
3.4 Summary.....	30
CHAPTER 4 SIMULATION SYSTEM SET UP	31
4.1 Initial Configuration Generation	31
4.2 System Equilibration	33
4.3 Crosslinking Reactions.....	35
4.4 Cooling Process	39

<i>4.5 Coating Testing and Quality Evaluation.....</i>	<i>40</i>
CHAPTER 5 CASE STUDY	45
<i>5.1 Material Specification.....</i>	<i>49</i>
<i>5.2 Base Case Analysis.....</i>	<i>50</i>
<i>5.3 Simulation Results.....</i>	<i>52</i>
<i>5.4 Summary.....</i>	<i>57</i>
CHAPTER 6 CONCLUSION	59
REFERENCES	62
ABSTRACT	66
AUTOBIOGRAPHICAL STATEMENT	68

CHAPTER 1

INTRODUCTION

This chapter will demonstrate a presentation on a current study on nanoparticle applied polymer coatings. This thesis attempts to provide a comprehensive review on nano coatings and will use Monte-Carlo simulation-based analysis technology to simulate the property change of polymer coating in curing and post-curing process.

1.1 Nanoparticle Applied Polymer Coatings

Nanoparticles are the particles between 1 and 100 nanometers in size. In nanotechnology, a particle is defined as a small object that behaves as a whole unit on its transport and properties (Dhoke et al., 2009). Nanoparticle research is currently an area of potential application in biomedical, optical and electronic fields. Nanotechnology application in coating field has shown remarkable growth in recent years. The incredible growth is because adding nanoparticle increases the availability of nanoscale materials like various types of nanoparticles, and advancement in processes can control coating structure at the nanoscale (Jalili et al., 2009). Through the study of the different type of nanoparticles in the past years, a list of properties that can be improved and the kind of nanoparticles suitable for the specific property improvements are shown in Table 1.

Table 1. Nanoparticle materials candidates for coating property improvement

Coating Property	Nanomaterial
Anti-microbial	CuO, TiO ₂ , ZnO
Gas Barrier	Nanoclays
Corrosion	Nanoclays, Boehmite
Electrical Conductivity, Static Charge Dissipation	ITO, ATO, SnO ₂
Fire Retardant	Nanoclays
IR-Absorption/Reflection	ITO, ATO, TiO ₂ , In ₂ O ₃
Magnetic	Fe ₂ O ₃
Mechanical, Scratch Resistance	Al ₂ O ₃ , SiO ₂ , ZrO ₂
Photocatalysis, Self-cleaning	TiO ₂ , ZnO
UV Stability	TiO ₂ , ZnO, BaSO ₄ , CeO ₂

Among these nanoparticles, silica has been widely used in the automotive field. As silica is the choice material of reinforcing transparent coating for applications like automotive top coatings, floor-wear layers, acrylic eyeglass lenses, and excellent scratch resistance enhancement (Yang et al., 2001). Scratch resistance is one of the most significant properties people are looking for since scratch can hardly be avoided in the product usage. The photochemical activity of nanoparticles like titanium dioxide plays a major role in the applications of coatings with them applied. Under the UV exposure and moisture, photoactive nanoparticles will provide and receive the energy, and their outermost electrons get activated. Electron transition occurs when electrons get enough energy, and this will make the H₂O transit to hydroxyl free radicals. After the photo-

initiated reactions get a significant conversion, top layers would degrade. During a water steam, this degraded layer will wash off with dirt collected, thus maintaining a clear appearance (Allen et al., 2002). Above is the principle of self-cleaning technique. However, since accelerated photodegradation is undesirable in most coatings, it becomes negative aspect in the application of photo-sensitive nanoparticles.

On the other hand, adding nanoparticles will make it even more difficult to analysis the coating's property regarding the cooperation between the poly matrix and nanoparticles. Also, nanoparticles will bring in new parameters such as type, size, load, etc. (Allen et al., 2004). In the following chapters, some research results will be carried out to present the effect of nanoparticles on the change of the property of coatings.

1.2 Polymer Coating Curing and Post-curing Process

Curing is a process where a polymer material is reacted to a highly cross-linked matrix system. After the polymer material is cured, physical properties will change, for example, hardness, brittleness, tensile strength, impact strength, etc. A curing process can occur at a room temperature, but for more quality products and faster curing speed, appropriate curing temperature can also be tested by Differential Thermal Analysis (DTA). Note that different curing agents work under different curing temperature conditions (Mirabedini et al., 2011). Recently, scientists and industries pay more attention to the post-curing phenomenon. As mentioned above, the curing process can happen at room temperature even the curing speed is extremely slow. In other words, after general industry curing process and products are exposed to the natural environment, a curing

process at an environment temperature is still in process. Therefore, to reduce the energy use, manufacturers attempt to not fully cure all coatings instead of a significant bond (Dhoke, et al., 2009). For some particular usage, manufacturers even expose products to natural environment without sending them to the curing oven. On the other hand, curing in the natural environment will cause incomplete curing and partial physical properties may not reach a criterion. Because of the existence of the post-curing phenomenon, it becomes difficult to estimate the product properties and functions properly. To generate a better quality control, a thorough understanding of the curing process is necessary.

1.3 Process Modeling and Simulation

Computational simulation is a technique for study curing process comprehensively. As scientists have made a significant effort on the mathematical description of polymer formulation, it becomes easier to use a computational method to recognize the chemical change procedure. Xiao (2009) has generated a Monte Carlo simulation methodology to simulate the effect of physical properties changes by the modification of nanoparticle applied thermoset polymer coating. With further development, the curing process can also be gained.

Another benefit that computational method provides is that with a comprehensive understanding of polymer material curing mechanism, it saves time and reduces material cost to predict products properties rather than through extensive experiments. Monte-Carlo simulation is a perfect match to simulate the curing and post-curing process.

1.4 Thesis Overview and Contributions

This thesis is organized in the following manner. Analyze effective parameters of nanoparticles applied coatings and state the advantages and challenges in Chapter 2. Summarize current simulation method of nanocoating in different structure level. Provide the computational design concept and process in Chapter 4. Verify and analyze the computational results in Chapter 5. Chapter 6 concludes the work, where future directions in this area are discussed.

In this thesis, recent research on the nanocomposites effect from category, shape and heterogeneity has been reviewed and analyzed. When nanocomposites bring significant functional improvement, it also leads post curing phenomenon. To have a better prediction and quality control for industry curing process design, a series of computational simulation work has been studied on. In order to simulate polymer network formulation process as far as possible, Monte Carlo simulation method is used in this work. By modifying the existed MC simulation procedure, a series of data and curves is provided.

Another contribution of this thesis is by using MC simulation method, a dynamic polymer components conversion change can be clearly seen. A dynamic properties change provides a more reliable and clear understanding on how curing speed changes in and out of a heating oven. For the coatings which designed to be used in normal temperature, this is a more visualized method to predict and redesign.

CHAPTER 2

PARAMETERIZATION FOR NANOCOATING SYSTEM

Scientific concepts regarding the benefits of controlling material in nanoscale have been around for half a century and nanotechnology was developed dramatically in the past decades as nanoparticle gain its popularity in the wide area.

Characterizing the property change of nano coating is always the hot topic that scientists focus on (Fufa et al., 2012). A lot of environment factors such as temperature, moisture, UV exposure intensity, etc. have been tested and studied. The effect of nanoparticles can be drawn from experiments results. Additionally, in modeling simulation technique, all effective factors should be considered to provide a comprehensive understanding and analysis, so valid clarifying parameters of nano coating is important in simulation work.

2.1 Effect of Nanoparticle Category

In coating area, many nanoparticles are studied to enhance the mechanical behavior such as scratch resistance. Among these nanoparticles, many categories can be divided based on the character such as specific property, structure, etc. To make more analysis, two classes are split in this research, one is nonmetallic oxide like silica, another is metallic oxides, such as TiO_2 , Al_2O_3 , Fe_2O_3 , etc.

Nano-silica is regarded as the most used nanoparticle in automotive coating because it can bring substantial enhancement in scratch resistance. The research results provided by Yari (2014) is shown in Figure 2.1.1. In a typical acrylic system, by adding 3.75% nano-silica, gloss retention

is improved to about 99% from 96% after 1000 hours artificial accelerated weathering conditions. On the other hand, the roughness ratio decrease is shown in Figure 2.1.2 (Yari et al., 2014), the hardness decreased to 1.5 from 4.4, by adding 3.75% nano-silica.

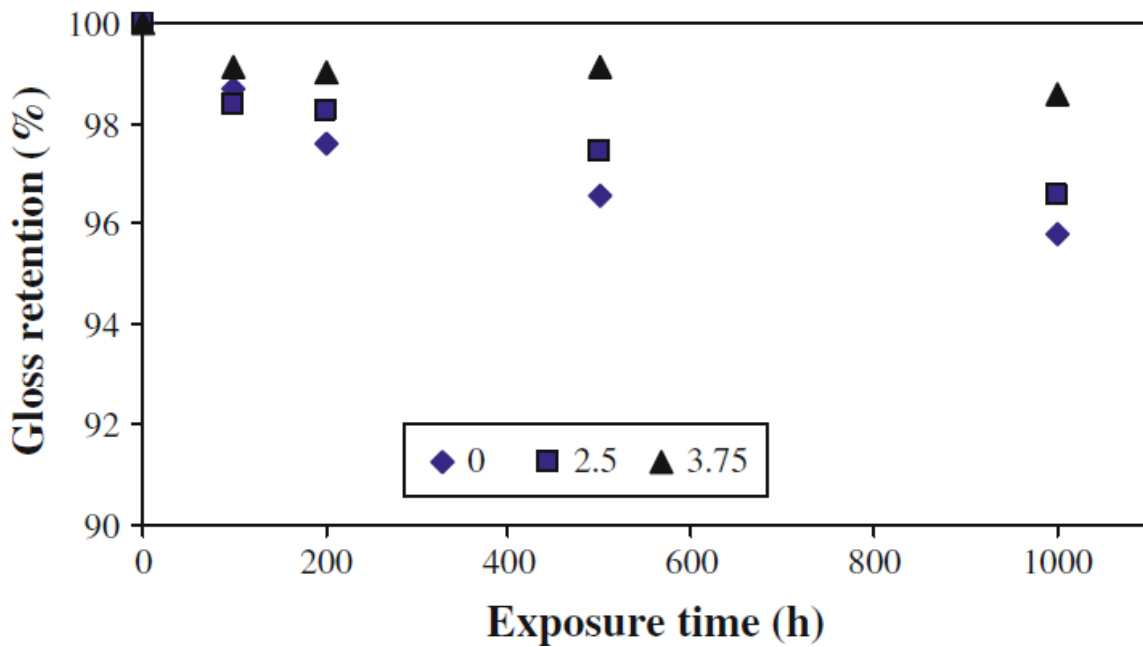


Figure 2.1.1 Gloss retention of clear coat containing different loads of nano-silica after various weathering times (Yari et al., 2014).

From their results, both gloss retention and roughness changes are modified towards more durable by adding different amounts of nano-silica after different periods of weathering exposure. These results may be due to the absorbance of nano-silica itself and scattered rays caused by particles that have been deviated from detector direction and considered as absorbance. Jalili (2009) has indicated that nano-silica can be regarded as photo-stabilizer in the photo-degradation. Nano-

silica absorbs and scatters some part of light from exposure environment. In other words, the coating itself acquires less degradation energy from the environment.

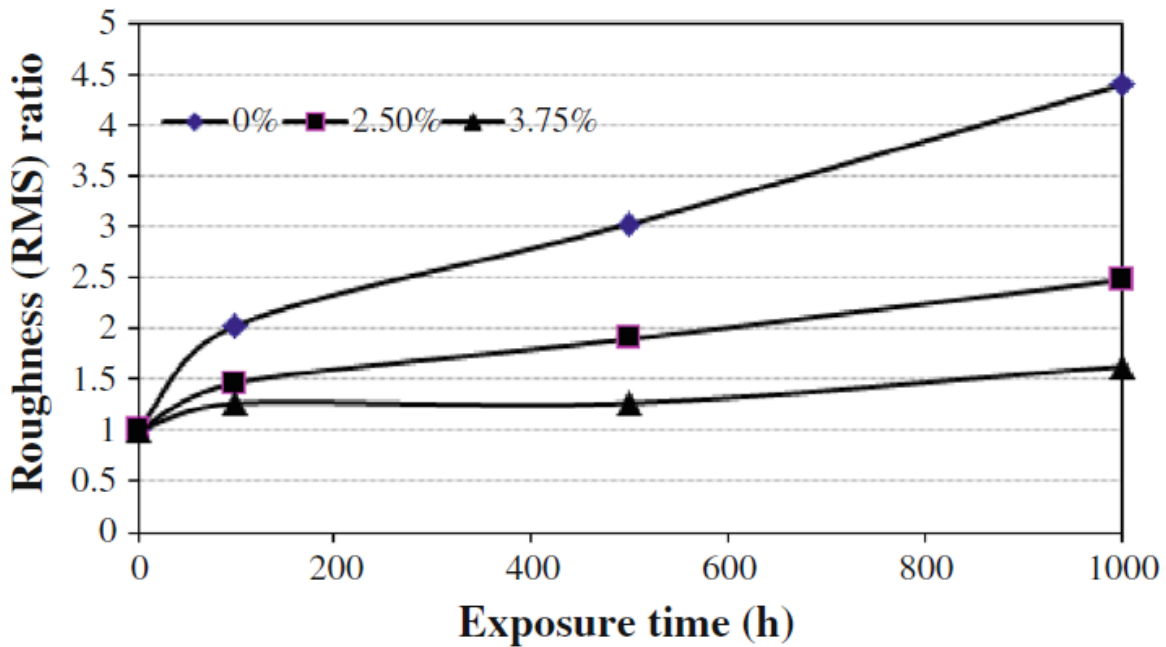


Figure 2.1.2 Roughness variation of different acrylic melamine clearcoat containing different loads of nano-silica during weathering (Yari et al., 2009).

Like coins have two sides, adding nano-silica reduces coating's crosslink density if curing process is not optimized. However, a post-curing phenomenon occurs during the exposure test. The crosslink density change in the exposure test is shown in Figure 2.1.3 (Yari et al., 2014). The crosslink density of pure acrylic decreases from 4.6 mol/m^3 to 2.2 mol/m^3 during 1000 hour exposure test, but because of the post-curing phenomenon, the crosslink density increases from 0.6 mol/m^3 to 2.3 mol/m^3 . This means a different curing operation may be needed to accomplish the curing process.

From Figure 2.1.3, it also can be seen that with nano-silica, the crosslink density is going higher during this 1000 hours exposure to weathering. However, the crosslink density of pure acrylic coating follows the typical scene decreasing from the very beginning (Fufa et al., 2013). This leads to two questions, 1) why crosslink density becomes lower than usual with nano-silica after cured? 2) What is the interaction between nano-silica and a conventional acrylic coating which makes crosslink density goes up?

A concept of post-curing is come up in nano technique. It explains the correlation between the base polymer layer and nanofillers. With nano-silica and the same curing process, the coating would not be fully cured as nanoparticles impede the cross-linking reaction which happens when double bond breaks under elevated temperature (Doh et al., 2008). In other words, under the same curing process, the curing process of coatings containing nanoparticles is uncompleted; note that uncompleted curing leads to a lower crosslink density at 0-hour exposure.

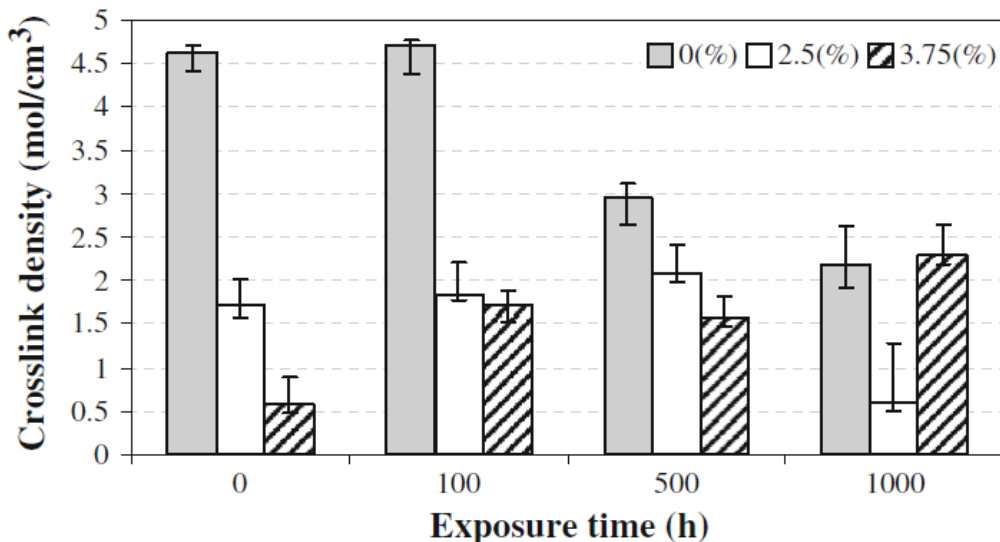


Figure 2.1.3 Crosslink density change after weathering with different loads of nano-silica (Yari et al., 2008).

Continually, when coatings are in use or exposed to nature environment, curing still takes place at environment temperature (Skaja et al., 2006). As a reciprocal effect of weathering exposure and post-curing, the crosslink density goes up in the 1000 exposure time with 3.75% nano-silica. However, with 2.5 % nano-silica, at around 500 exposure time, the crosslink density gets its peak value, and after that, the crosslink density goes down as usual (Rajagopalan and Khanna, 2013). This is because weathering degradation takes advantage of the reciprocal effect. Therefore, even a further result is not shown in their research; it is reasonable to deduce that with a higher load of nano-silica, the crosslink density will still decrease after reaching a significant time.

Furthermore, further results from DMTA and FTIR also show that, before exposure, the nano-silica containing clear coats had lower crosslink density compared to the pristine clear coat, indicating an uncompleted curing process for these coatings (Yari et al., 2014). For another

category, metallic oxide, many researchers have made their effort on TiO_2 , Al_2O_3 , Fe_2O_3 , ZnO , etc. Shailesh (2009) did a study of the effect of nano-size Al_2O_3 , Fe_2O_3 , ZnO on the alkyd-based waterborne coating system. During the research, Yari (2014) did a lot AFM and SEM observation under different test content. In various exposure conditions which are unexposed, salt spray, humidity, UV, with the load of nano-size Al_2O_3 , Fe_2O_3 , ZnO increases, coatings always show a better performance. For example, from the AFM result of UV, the AFM value decreases to 10.790 from 35.935 for neat alkyd-based waterborne coating.

Finally, a conclusion was drawn, the effect of nano-size Al_2O_3 , Fe_2O_3 , ZnO addition on the corrosion, mechanical and optical properties of the alkyd-based waterborne coating was investigated (Ahmadi et al., 2007). It was found the addition of small concentration of nano-size Al_2O_3 , Fe_2O_3 , ZnO can improve the corrosion resistance, scratch resistance and abrasion resistance of the coating to a better extent. Moreover, the addition of nano-size Al_2O_3 , Fe_2O_3 , ZnO showed no disturbance to optical transparency of the layer, instead had provided strength to the polymer composite preventing it from photo-degradation (Yari et al., 2012). Also, small loading level of nano- Al_2O_3 , Fe_2O_3 , ZnO in the coating system decreases the curing temperature as compared to the clean surface thereby improving its curing and film forming properties.

2.2 Effect of Nanoparticle Shape

Nano-size ZnO was studied in epoxy coating system with regarding flake-like nano- ZnO and spherical nano- ZnO (Rajagopalan and Khanna 2013). In their study, samples were exposed to accelerated weathering chamber and color change dE and yellowness index was measured. By the

figure they gave below, the relationship between the shapes of nano particles and coating property can be clearly seen.

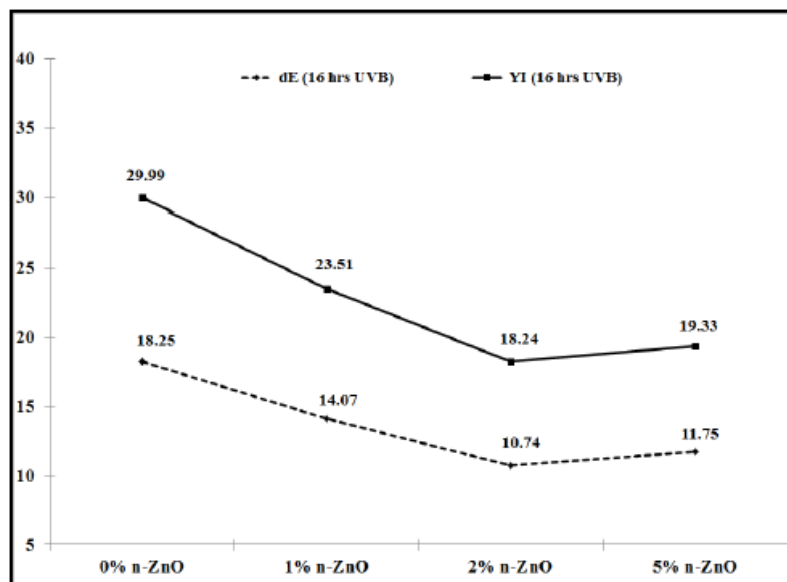


Figure 2.2.1 Color change and yellowness index after 16 hrs exposure respect to different percentages of flake-like ZnO load (Rajagopalan and Khanna, 2013).

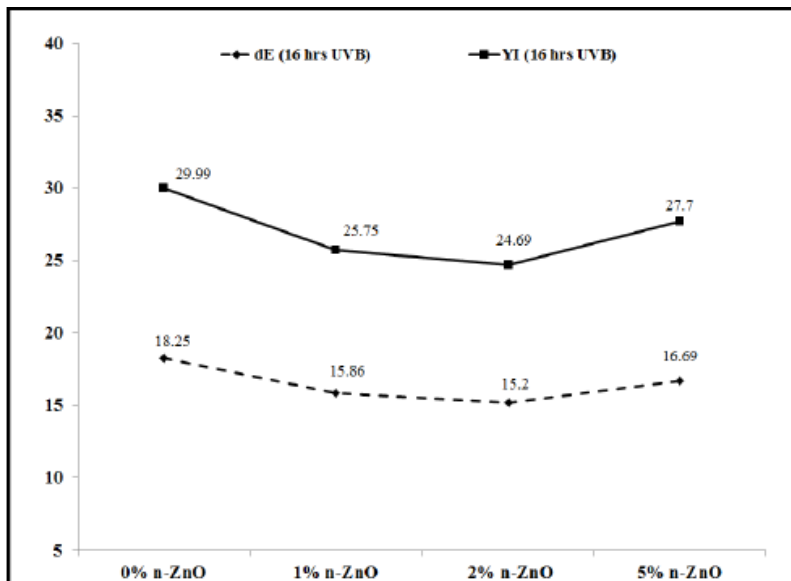


Figure 2.2.2 Color change and yellowness index after 16 hrs exposure respects to the different proportion of spherical ZnO amount (Rajagopalan and Khanna, 2013).

From the comparison of Figure 2.2.1 and 2.2.2 (Rajagopalan and Khanna, 2013), flake like ZnO always presents a better performance on color change resistance and yellowness with different weight percentage. Even spherical ZnO also improves the optical property, but flake-like ZnO works more efficient than spherical shape according to the data shown above. High rate reduction values in dE and YI indicates more resistance to color change and yellowing (Yari et al., 2014). The highest percentage reduction values were observed at 2% loading level respectively for flake-like and spherical nano-ZnO modified epoxy coatings compared to 1% and 5%. Flake-like nano-ZnO reduced color change and yellowing by 40% while spherical nano-ZnO reduced the same by 17%, at 2% loading in the coating formulation.

However, with the load percentage increases, the color change resistance, and yellowness resistance slightly lowered. This may because ZnO plays a role of photo-catalyst after a significant

proportion (Ortelli et al., 2014). Before that, the cooperation between photo-catalyst and light scatter works a decisive role. ZnO is regarded as a photo-catalyst during hydrolysis reactions. Hydroxyl free radical is produced during the hydrolysis reaction and will damage organic structures. Producing hydroxyl free radical and reacting with polymer structure is a mechanism of the self-cleaning property of nano-ZnO.

2.3 Effect of Nanoparticle Heterogeneity

Even though nanoparticles are defined as particles between 1 to 100 nanometer in size, there is still a lot of value to study the heterogeneity effect on the physical properties, particularly for metallic nanoparticles like TiO₂ that have different crystal types such as anatase and rutile. Research has shown that even in nano-size, particles still works differently respect to their crystal form (Xiao et al., 2010). The research carried out by Peng (2014) stated the relationship between acrylic urethane coating properties and nano-TiO₂. TiO₂ is selected in their study, because TiO₂ is a photoreactive material with a different level of photoreactivity that depends on its crystal type: anatase and rutile. In their study, three types of TiO₂ crystal form were studied with similar crystal size but a different level of photoreactivity, an anatase form (P_C), a rutile form (P_B) and a mixed crystal form of both anatase and rutile (P_A). Four groups of samples were selected to take an artificial accelerated weathering test; they were a group of pure anatase, a group of pure rutile, a group of mixed of anatase and rutile and unfilled acrylic urethane (Kiil, 2012). After the exposure test respecting different crystal type, another exposure test was followed up for studying the effect of moisture in the testing environment.

From the RMS surface roughness results which are presented in Figure 2.3.1 (Peng, 2014), three stages are shown. No significant changes in roughness were observed in the first stage (before t_1); this is because only the erosion of the thin clear layer took place (Kiil, 2013). The thin clear layer is a region which only contains pure AU material and will photo-degrade before nano-TiO₂ play a part in. In the second stage (between t_1 and t_2), roughness increased dramatically due to the development of a network-like structure formed during polymer degradation around particle agglomerates. In the third stage (after t_2), the roughness increased slowly, probably because of a very slight change in topographical structure (Gu et al., 2012). It might be related to the shielding effect of the densely and uniformly distributed PA nanoparticles on the surface. For AU-PC coating under the wet condition (indicated by dotted lines in Figure 2.3.2 (Peng, 2014)), the RMS roughness curve can also be divided into three stages. In the first stage (before t_1'), no obvious changes were observed, due to the erosion of the thicker clear layer. In the second stage (between t_1' and t_2'), the roughness increased slowly, due to the formation of some pits around the particle clusters. In the third stage (after t_2'), the roughness increased dramatically, due to growing and merging of the pits and the severe degradation around the large particle clusters (Pickett et al., 2009).

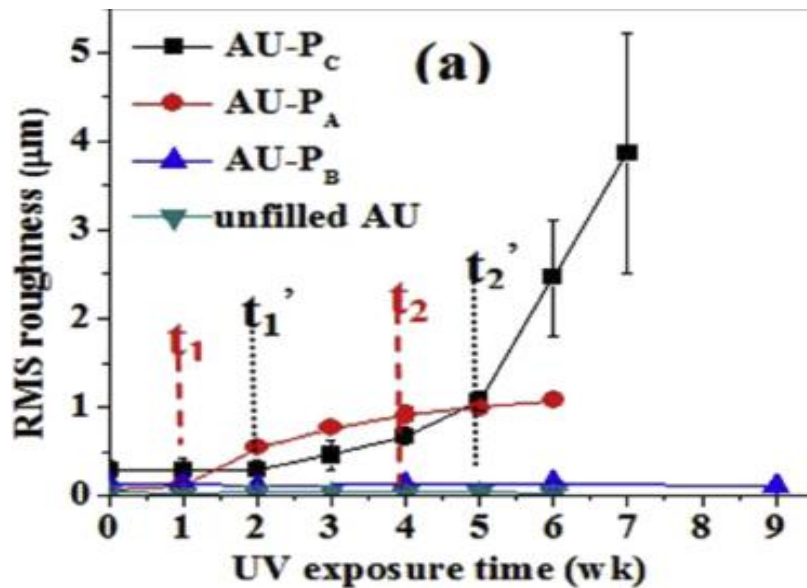


Figure 2.3.1 RMS roughness change respect to exposure time with different TiO₂ crystal type

(Pang et al., 2014).

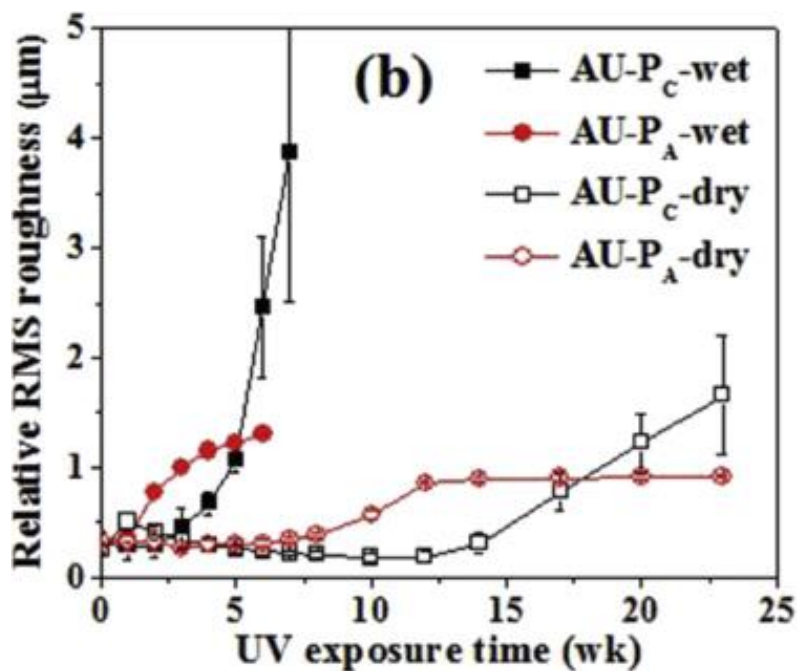


Figure 2.3.2 RMS roughness change respect to exposure time with different TiO₂ crystal type

and exposure RH (Pang et al., 2014).

Another observation focusing on the effect of moisture was followed up. A mix of both anatase and rutile (P_A) and pure rutile (P_C) were picked out under different exposure relative humidity (dry: 30°C, 0% RH; wet: 30°C, 75% RH) and the results can be seen in Fig. 2.3.2.

The results clearly present the effect of moisture. No matter observing AU- P_C or AU- P_A , the roughness change in higher humidity is much more dramatically than that in lower humidity (Pang et al., 2014). This may be caused by the photo-catalyst property of TiO_2 . Much research has indicated that TiO_2 plays a role of a photocatalyst in the cooperation in coatings. Nano-size TiO_2 can slowly react with moisture under UV radiation and produce hydroxyl free radical ($\cdot OH$). Hydroxyl free radical has extremely high oxidizing property only after fluorine-free radical in nature. The same function as ZnO , TiO_2 has the same property of self-cleaning, but this oxidizing damaging function is unrecognizable, which means the high oxidizing free radical will also damage polymer coating itself and accelerating the photodegradation (Dhoke et al., 2009).

2.4 Challenges

The critical challenges of nanotechnology growth have four categories: 1) Material cost, 2) Dispersion, 3) Characterization, 4) Health and Safety. As nanotechnology develops, the material cost slowly decreases due to the increasing number of nanoparticle suppliers, improved manufacturing method, and increasing sales volumes (Jalili and Moradian, 2009). Nanoscale dispersion is critical for realizing the potential benefits of incorporating nanoparticles in coatings. Early attempts to commercialize nano- TiO_2 were unsuccessful because of the high degree of

agglomeration of the powder and subsequent difficulties in re-dispersing the particles in coatings. A recent review of the challenge of dispersion of nanoparticles in polymeric systems concluded that virtually all systems examined, regardless of the nanoparticle chemistry or the shape (spherical, rod-like, platy, etc.), a large-scale poorly dispersed material was present.

One approach to achieving nanoscale dispersion is to use effective grinding methods such as ball milling (Yang et al., 2001). Effective dispersing requires grinding media that is much smaller than those used for dispersing conventional particles. The high surface area of dispersed nanoparticles can significantly increase the dispersant demand. High viscosity caused by finely dispersed nanoparticles is another problem that needs to be addressed. The large surface area can increase viscosities due to the increase in interfacial forces (e.g., electroviscous forces) and limit the number of nanoparticles that can be incorporated. Adding the right surface functionality to address dispersibility and viscosity rise is another approach to addressing dispersion issue. In addition to promoting dispersion, functionalizing the particle surface enables the nanoparticle to be covalently linked to the organic resin matrix.

Characterization of nanoscale particle dispersion and nanostructure requires techniques that are not common in a small to mid-size coating manufacturer's research and development laboratory (Allen et al., 2002). Surface characterization requires techniques such as Scanning Probe Microscopy (SPM) (e.g. Atomic Force Microscopy) and Scanning Electron Microscopy (SEM). Film cross-sectional analysis requires techniques such as Transmission Electron Microscopy (TEM), SEM, X-ray and neutron scattering. Although certain nanomaterials have been commercially used for many decades (e.g. colloidal silica and carbon black), commercialization of new nanomaterials has outpaced the development of their safe handling

methods (Allen et al., 2004). The awareness of the need to understand both short- and long-term effects of nanomaterials heightened in recent years. In 2006, the European Center for Ecotoxicology of Chemicals (ECETOC) published the results of a review of the potential risks of nanomaterials. The US Environmental Protection Agency (EPA) in early 2008 launched the registry of TSCA inventory status of nanoscale substances.

2.5 Overview

Nano techniques have been developed over the past decade. From what has been discussed above, researchers and industries are interested in utilizing and producing proper nanocoating. Consequently, testing and optimizing the effect and side effect from nano particles are necessary. Also, part of parameters such as type, shape, heterogeneity, etc. are studied by experiments and computational methods, and the essential effects of nanoparticles have been well studied (Mirabedini et al., 2011). Nanoparticles mostly bring positive functional enhancement in a different area. However, there is not a comprehensive methodology that can provide a coverage of all polymer coatings and nanoparticles system because the interaction between polymers and nanoparticles are different and complicated. As discussed above, one of the most critical nanoparticle issues in production and quality control is Post-curing. Applying nano particles will significantly increase the difficulty of controlling product quality and properties. Even though the product properties can be tested by experimental methods, computational simulation can also bring in a more comprehensive method for property prediction with less time and cost (Dhoke et al., 2009).

In the next chapter, three computational simulation methods will be introduced for fulfilling different analysis demands. By comparing and analyzing these current computational methods, a more suitable method will be chosen to analyze product curing and post-curing process.

CHAPTER 3

COMPUTATIONAL SIMULATION METHODOLOGY

To fully characterize the physical properties of nanocoatings, either in use or before use, comprehensive modeling must consider large factors and be able to describe nano coatings in 3D space of computational conditions and quantify the interaction between polymers and nanoparticles. In other words, the significant task of computational design is to establish extensive connections between nano-component, processing conditions, coating microstructure, property, and performance (shown in Figure 3.1 (Xiao et al., 2009)).

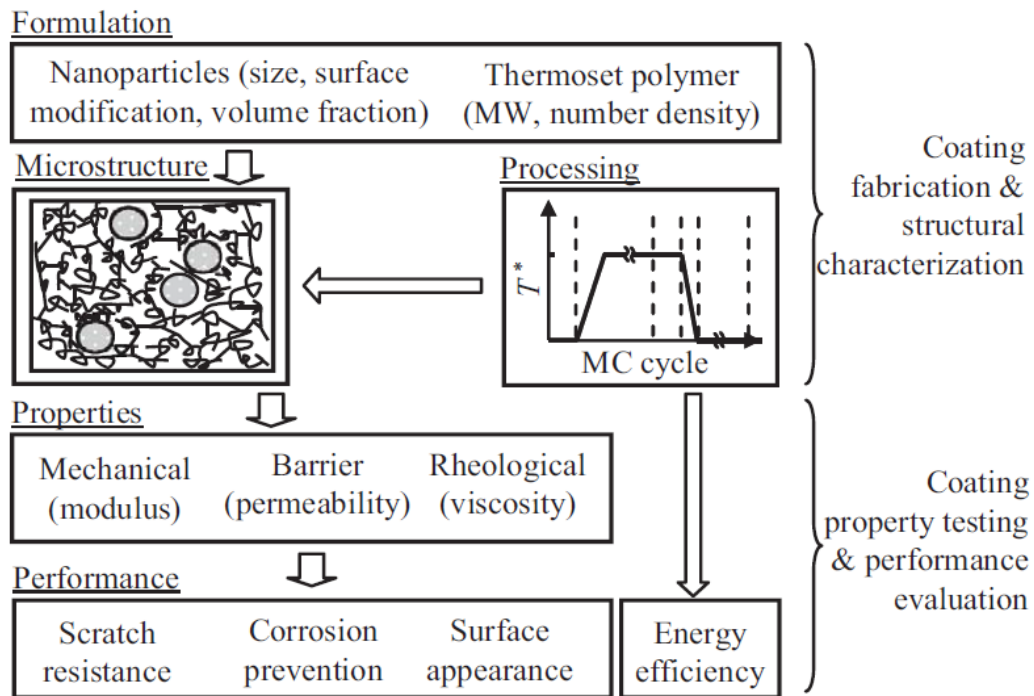


Figure 3.1 Multi-Scale Correlation establishment for Thermoset Nanocomposites (Xiao et al., 2009).

3.1 Off-Lattice Simulation

Xiao (2009) has developed a series of off-lattice simulation method for thermoset nanocomposites. In his simulation work, a nanoparticle dimensional determination simulation box coating is formed to simplify the simulation work because to simulate the whole nano coating will dramatically increase the computational time of the simulation work and in a polymer structure; the partial component has not a huge difference with the entire coating system (Fufa et al., 2012). On the other hand, in this case, off-lattice Monte Carlo simulation method is more suitable than Molecular Dynamics simulation because Monte Carlo simulation can satisfy both the demand of time scale and length scale. Monte Carlo simulation has its time scale of about 10^3 s and for Molecular Dynamics simulation, the time scale is about 10^{-15} s (Xiao et al., 2010). On the other hand, Monte Carlo simulation, in this case, is able to study system that contains long chains and large particles which are bigger than 10σ . The simulation box is determined as a cubic.

The total number of nanoparticles (N^n) can be described as:

$$N^n = \text{int} \left(\frac{3\phi^n(N^m + N^c)}{4\rho^p(1-\phi^n)\pi(R^n)^3} \right) \quad (3.1.1)$$

where ρ^p is the number density of polymer materials and N^m and N^c are respectively the total number of effective monomers and crosslinkers; R^n and ϕ^n are respectively the volume fraction of nano particles (Xiao et al., 2010). The edge length of a cube simulation box can be calculated as:

$$l_0^x = \sqrt[3]{\frac{N^n 4\pi}{3\phi^n}} R^n \quad (3.1.2)$$

For convenience, the entity numbers from 1 to N^m are reserved for N^m effective monomers, the number from $N^m + 1$ to $N^m + N^c$ are provided to N^c crosslinkers, and the number from $N^m + N^c + 1$ to $N^m + N^c + N^n$ are assigned to N^n nanoparticles.

To generate the first system configuration, all entities including nanoparticles, precursor polymer chains, and crosslinkers should all be placed into the simulation box. Additionally, according to Kremer and Grest (1990), the placement should satisfy three restrictions: 1) the distance between any two adjacent entities should be sufficient to avoid an extraordinarily high steric repulsion in between, 2) the distance between any two polymer beads must not exceed the maximum bond length, 3) polymer chain back folding must be prevented from separating every other polymer bead in the same precursor polymer chain so that the distance in between can be larger than a preset minimum distance (l_{min}^{bf}). With these three restrictions, a right polymer chain persistence length can be ensured (Kremer and Grest, 2009).

Additionally, to reduce computational time for achieving a system equilibration, all the bonds have the same initial length l_0^b . With previous three restrictions, these four restrictions are enough for generating an initial system that is close to equilibrium. Three system equilibrations are reached in the coating sample development. The first is the equilibration that occurs after an initial configuration is generated (Xiao et al., 2010). The second is after the cross linking reaction. The third is needed after the coating is cooled. With satisfying these three equilibration request, system states can be described through computational simulation.

Moreover, the Metropolis algorithm is directly adopted in the simulation (Metropolis et al., 1953). By this method, system microstructure evolution is realized through generating a Markov

chain of configurations (Allen and Tildesley, 1987). The probability of accepting a trial configuration in the Markov chain can be expressed as (Allen and Tildesley, 1987)

$$p = \min \left\{ 1, \exp \left(- \frac{\Gamma^{trial} - \Gamma^{now} + P(V^{trial} - V^{now})}{k_B T} \right) \left(\frac{V^{trial}}{V^{now}} \right)^{N^e} \right\} \quad (3.1.3)$$

Through his work, several properties are simulated such as scratch resistance, energy efficiency, polymer-bead cumulative number percentage distribution, and crosslink density distribution (Gu et al., 2012). His simulation work is probably the first methodology which uses Monte Carlo simulation in 3D polymeric system. His work helps people to gain a broad and comprehensive standing for the interaction between polymeric material and nano-component.

3.2 Kinetics Simulation

Monte Carlo simulation has its own advantages like time and length scale, random placement mechanism which is regarded as more similar to national polymeric formulation mechanism (Pickett et al., 2009). However, for long-term prediction, this method has its limit because this methodology does not contain an in-use process simulation; even Molecular Dynamics has a smaller time scale. A kinetics simulation method is necessary for a long-term prediction case because by computational calculation, the partial differential equation of chemical kinetics can be easily gained.

Kiil (2013) developed a mathematical model based on the kinetics of the degradation process of polymer material with nano-component. In his work, epoxy-amine is the polymeric component that is focused. The first concept came up with is “oxidation zone” (shown in figure 3.2). Based on the oxygen diffusion ability, they assumed that coating oxidation reaction only takes

place in the oxidation zone which contains oxygen, and out of this oxidation zone, since oxygen does not exist, polymer stays inactive state (Kill, 2013).

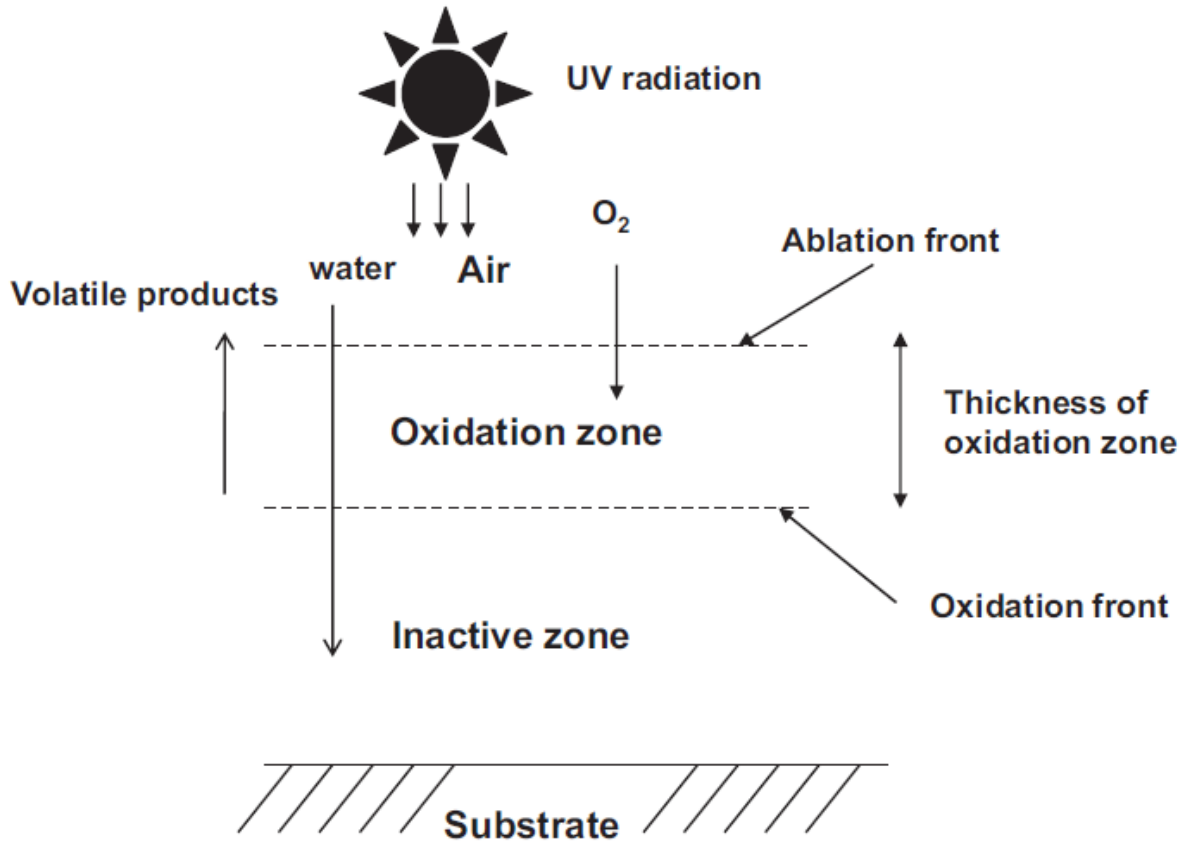


Figure 3.2 Schematic illustrations (cross-section view) of the epoxy-amine coating during exposure to ultraviolet radiation and humidity (Kiil, 2009).

Here, ablation front is the front that reaches a significant conversion, and oxidation front is the division of oxidation zone and inactive zone. Since for the ablation front, the conversion is regarded as unchangeable with both time and position, which can be described as:

$$\frac{dX_{CL}}{dt} = \left(\frac{\partial X_{CL}}{\partial t}\right) dt + \left(\frac{\partial X_{CL}}{\partial L}\right) dl \quad (3.2.1)$$

where X_{CL} is the conversion of epoxy chains in the epoxy-amine network.

With rearrange the equation, the position of ablation front can be expressed as:

$$\frac{dl_A}{dt} = \frac{-\left(\frac{\partial X_{CL}}{\partial t}\right)\big|_{l=A}}{\left(\left(\frac{\partial X_{CL}}{\partial t}\right)\big|_{l=A}\right)_t} \quad (3.2.2)$$

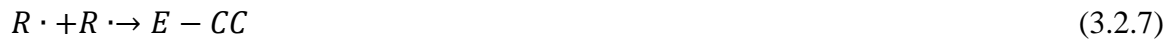
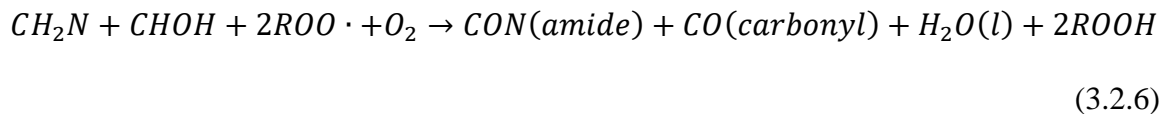
where l_A is the position of moving ablation front.

For oxidation front, since the change of concentration of oxygen is regarded as unchangeable, the position of oxidation front can be expressed as:

$$\frac{\partial C_{O_2}(l,t)}{\partial l}\bigg|_{l=l_A} = 0 \quad (3.2.3)$$

where C_{O_2} is the concentration of oxygen.

After determining the simulation system, a series of chemical kinetics equations must be ensured. The degradation process can be expressed as below:



where $E - CC$ is the epoxy-amine component; $R \cdot$ and $ROO \cdot$ are activated intermediate products.

Then based on the fixed degradation process, kinetics can be drawn as blow:

$$-r_1 = k_1 E_r^{\frac{1}{2}} C_{CC} \quad (3.2.9)$$

$$-r_2 = k_2 [R \cdot] C_{O_2} \quad (3.2.10)$$

$$-r_4 = k_4[R \cdot]^2 \quad (3.2.11)$$

$$\left(\frac{\partial C_{cc}}{\partial t}\right)_l = -(-r_1) + (-r_4) \quad (3.2.12)$$

$$\left(\frac{\partial [R \cdot]}{\partial t}\right) = (-r_1) - (-r_2) - (-r_4) \quad (3.2.13)$$

where C_{cc} , C_{O_2} are respectively the concentration of group CC and oxygen; $[R \cdot]$ and $[\cdot OH]$ are the dimensionless concentration of activated free radical intermediary $R \cdot$ and hydroxyl; r_1, r_2, r_4 are the reaction rate of each reaction and k_1, k_2, k_4 are the reaction constant for reaction 1, 2, 4 respectively. E_r Is the radiation intensity of the transmitted light at the reaction position.

By solving the partial differential equations, the concentration of each critical component can be easily obtained; additionally, the position of ablation front and oxidation front can be simulated too. From the simulation results, an oxidation zone is clearly shown. After about 6 days, the movement of oxidation front and ablation front becomes parallel, which means there is a fixed width zone that exists when the coating is exposed to UV radiation (Yang et al., 2001). The oxidation zone is about $2\mu\text{m}$. With the results shown in their work, the thickness of the epoxy-amine coating will reduce about $6.7\mu\text{m}$ after 50 days UV radiation. The mass loss of the polymer coating is about -4.6% after 50 days UV radiation.

In the following study carried out by Kiil (2009), the light stabilizer is added to the simulation system. With using the same method, not only the previous results can be gained, the concentration of light stabilizer can be achieved either. Since the reactions between TiO_2 and the polymeric system is tested and theoretically as long as we know the reaction constants and the scatter effect on the radiation intensity (E_r), the in-use property change is able to be simulated (Kiil, 2012).

This chemical kinetics simulation provides a general concept of in-use polymer concentration and physical property change. A long-term over ion performances predict is also provided by this method. However, it is still far from reality use situation as the natural conditions are still different for individual sample and undesirable damage to flying stone, car wash, etc. may happen (Pickett et al., 2009). Comparing these two simulation methods, both of them provide a more comprehensive understanding of nano-component in a different stage and each of them has its own advantages and focus. Monte Carlo method can simulate formulation process and analysis the effect of size, nano-component volume fraction, etc. and kinetics method can provide a longer prediction.

3.3 Potential Energy Models

Kremer and Grest (1990) have introduced a coarse-grained beaded spring model. In their work, they assume that polymer beads are in the same size, and between each bead, a reaction created bond connects an effective monomer and a cross-linked by the same type of spring in precursor polymer chain.

The potential energy between two polymer beads can be expressed as

$$\Gamma_{i,j}^I = 4\varepsilon^{pp} \left(\left(\frac{\sigma}{r_{i,j}} \right)^{12} - \left(\frac{\sigma}{r_{i,j}} \right)^6 \right) \quad r_{min}^{pp} \leq r_{i,j} \leq r_{max}^{pp} \quad (3.3.1)$$

where $r_{i,j}$ is the distance between beads i and j ; ε^{pp} is an energy parameter; σ is a distance parameter; r_{min}^{pp} and r_{max}^{pp} are respectively the minimum distance and the cutoff distance between any two non-bonded polymer beads.

Additionally, the potential energy equals to zero when the distance between two beads is larger than the cutoff distance (Pang et al., 2014).

The potential energy of two bonded beads I and j can be adjusted by the finite extension nonlinear elastic potential and the LJ potential (Kremer and Grest, 1990), which provides

$$\begin{aligned} \Gamma_{i,j}^{\text{II}} = & -\frac{\mu\varepsilon^{pp}}{2\sigma^2} (l_{max}^b)^2 \text{In} \left(1 - \left(\frac{r_{i,j}}{l_{max}^b} \right)^2 \right) \\ & + 4\varepsilon^{pp} \left(\left(\frac{\sigma}{r_{i,j}} \right)^{12} - \left(\frac{\sigma}{r_{i,j}} \right)^6 \right) \quad r_{min}^{pp} \leq r_{i,j} \leq l_{max}^b \end{aligned} \quad (3.3.2)$$

where μ is a spring constant, l_{max}^b is the maximum allowable bond length.

For single spherical beads which are connected by a polymer bead and a nanoparticle is introduced by Vacatello (2001, 2002), which provides

$$\Gamma_{i,j}^{\text{III}} = 4\varepsilon^{pn} \left(\left(\frac{\sigma}{r_{i,j}-R^n} \right)^{12} - \left(\frac{\sigma}{r_{i,j}-R^n} \right)^6 \right) \quad r_{min}^{pn} \leq r_{i,j} \leq r_{max}^{pn} \quad (3.3.3)$$

where ε^{pn} is an energy parameter which is determined by the size ratio of the nano particle and the polymer bead; R^n is the nanoparticle radius; r_{min}^{pn} and r_{max}^{pn} are respectively the minimum distance and the cutoff distance between a nano particle and a polymer bead.

Similarly, the potential energy between two nanoparticles is adjusted as

$$\Gamma_{i,j}^{\text{IV}} = 4\varepsilon^{nn} \left(\left(\frac{\sigma}{r_{i,j}-2R^n} \right)^{12} - \left(\frac{\sigma}{r_{i,j}-2R^n} \right)^6 \right) \quad r_{min}^{nn} \leq r_{i,j} \leq r_{max}^{nn} \quad (3.3.4)$$

where ε^{nn} is an energy parameter; r_{min}^{nn} and r_{max}^{nn} are respectively the minimum distance and cut-off distance between tow nano particles.

Four potential energy between, two non-bonded polymer beads, two bonded polymer beads, polymer bead and nanoparticle bead. Two nanoparticles are well studied in the past decades. Potential energy is significant for studying the interactions in nanocoatings.

3.4 Summary

In this chapter, three modeling simulation methodologies are introduced. Each of them focuses on different structure levels, microcosmic and macroscopic, static and dynamical, before use and after use (Xiao et al., 2010). Based on these simulation methods, it is possible to provide more comprehensive analysis on an accurate system. Additionally, with the development of nanotechnology and model analysis methodology, using modeling method to analyze and predict the change of coating product containing nanoparticles becomes a hot topic in the recent research area. Theoretically, using off-lattice simulation and potential energy models, a series of models focusing on the curing of polymer coatings containing nanoparticles in ideal conditions can be provided and simulated.

CHAPTER 4

SIMULATION SYSTEM SET UP

As there is a huge demand for the definitiveness of coating properties in the procedure of curing and post curing, Monte Carlo simulation methodology will be introduced with detailed steps and explanations. These simulation steps from Xiao (2009) are consulted.

4.1 Initial Configuration Generation

As discussed in the last chapter, four restrictions should be considered when processing entities. In order to meet the constrictions, placement follows the procedure below:

Step 1: Place the first polymer bead randomly in a suitable place in the simulation box.

Step 2. Identify the next polymer bead with satisfying the following restriction vector equation:

$$r_i = r_{i-1} + \Delta r \quad (4.1.1)$$

where r_{i-1} the position vector of previous bead is, Δr is the relative position to the current placing bead. $\Delta r = (l_0^b \sin\theta_1 \cos\theta_2, l_0^b \sin\theta_1 \sin\theta_2, l_0^b \cos\theta_1)$. θ_1 And θ_2 are two random numbers between 0 and 2π .

If the placement success, jump to Step 4; if not continue to Step 3.

Step 3. Check if the number of placement is larger than the preset limit. If yes, this means the current placing bead is out of the queue, return to Step 2. If not, continue another attempt.

Step 4. Check if all beads in this chain have been placed. If yes, return to Step 2. If not, proceed to Step 5.

Step 5. Check if all chains in the queue have been placed. If yes, return to Step 1. If not proceed to Step 6.

Step 6. Place all polymer beads in the box to the available position.

Through these 6 steps, we can make sure that all polymer beads and chains in the queue are all placed in the right place and satisfy all these constrictions.

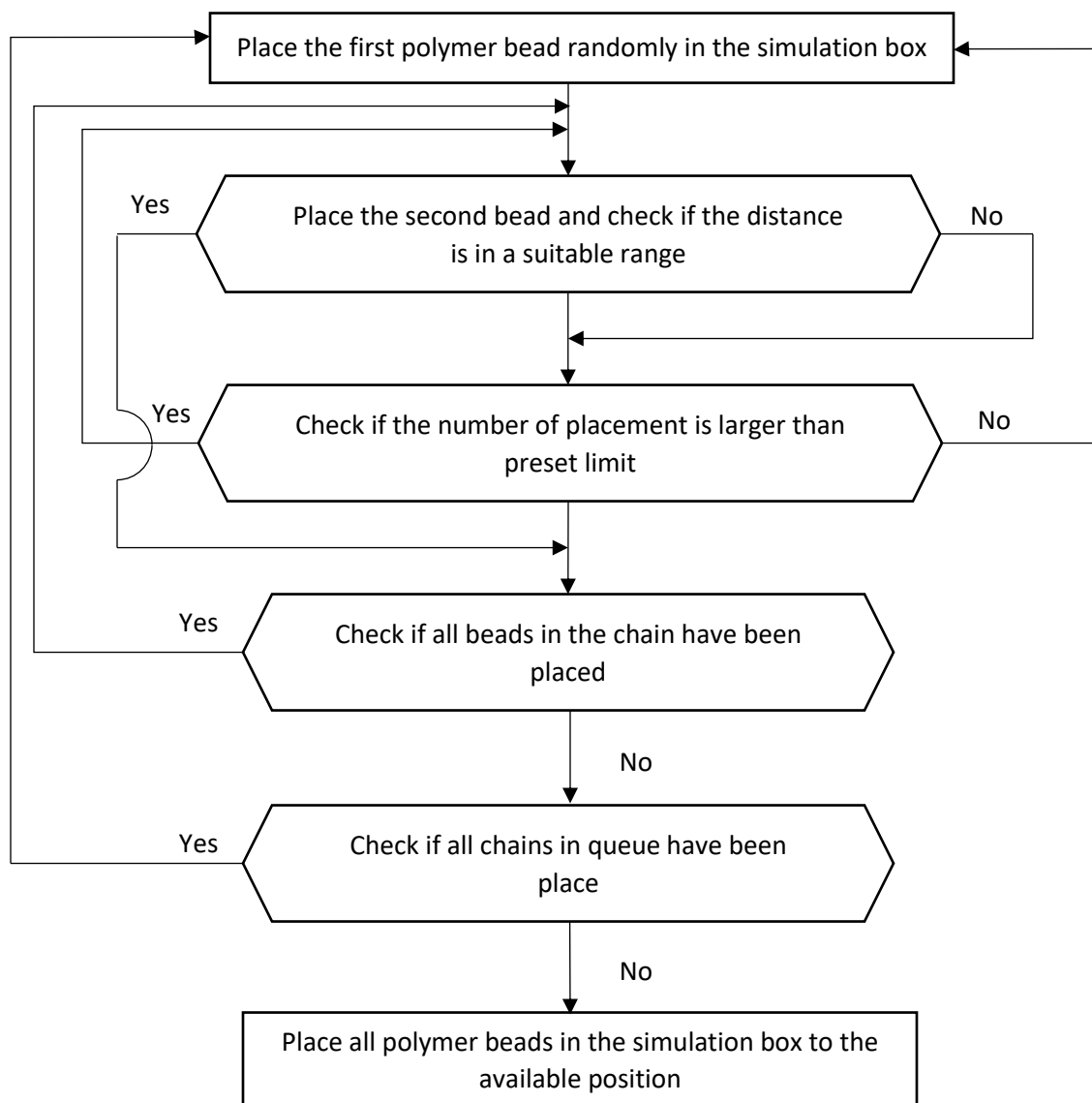


Figure 4.1 System initializing flowchart.

4.2 System Equilibration

As mentioned earlier, there are three system equilibrations that system must reach during this simulation. This equilibration can be finished by the following procedure:

Step 1. Initialize an equilibration process by setting the MC cycle index (I) to 0, and enter system temperature T , pressure P , and volume V .

Step 2. Start a new MC cycle by setting $I=I+1$.

Step 3. Attempt to displace all entities by following the sub-steps below:

Step 3.1. Initiate a new MC step and select randomly an entity that has not been selected in the current MC cycle. The position of the entity (the i th) is r_i .

Step 3.2. Determine a new position for entity i to move. The attempted new the position is provided by the vector r^{trial}

$$r_i^{trial} = r_{i-1} + \Delta r \quad (4.2.1)$$

and

$$\Delta r = (l_{i,max}^b \zeta \sin \theta_1 \cos \theta_2, l_{i,max}^b \zeta \sin \theta_1 \sin \theta_2, l_{i,max}^b \zeta \cos \theta_1) \quad (4.2.2)$$

where ζ is a random number between 0 and 1; $l_{i,max}^b$ is a maximum displacement distance for entity i in an MC step.

Step 3.3. Reject this move attempt and go to Step 3.5, if it violates either the minimum distance restriction or the bond length restriction; otherwise, continue.

Step 3.4. Move the entity to the new position, if the attempt is accepted according to the Metropolis criterion in Eq. (5); otherwise, this step attempt must be discarded.

Step 3.5. Check if all the entities have been sought to displace once in the current

MC cycle. If yes, go to Step 4; otherwise, return to Step 3.1.

Step 4. Attempt to change the volume of the simulation box by following the sub-

steps below, if the system is in an NPT ensemble; otherwise, go to Step 5 directly.

Step 4.1. Determine the new volume of the simulation box according to

$$V^{trial} = (\sqrt[3]{V^{now}} + l_{max}^v(2\zeta - 1))^3 \quad (4.2.3)$$

where l_{max}^v is the maximum length change of each edge of the simulation box in an MC step.

Step 4.2. The trial positions of all the N^e entities are recalculated as

$$r_i^{trial} = r_i \left(\sqrt[3]{\frac{V^{trial}}{V^{now}}} \right), i = 1, 2, \dots, N^e \quad (4.2.4)$$

Step 4.3. Reject the volume change attempt and go to Step 5, if it violates either the minimum distance restriction or the bond length restriction; otherwise, continue.

Step 4.4. Modify the simulation box volume and move all the entities to the new positions, if the attempt is accepted according to the Metropolis criterion in Equation.3.1.3 ; otherwise, this volume change attempt must be discarded.

Step 5. Check if the number of MC cycles has reached the preset maximum number (N_{Max}^{MCC}). If yes, the equilibration process is finished; otherwise, return to Step 2.

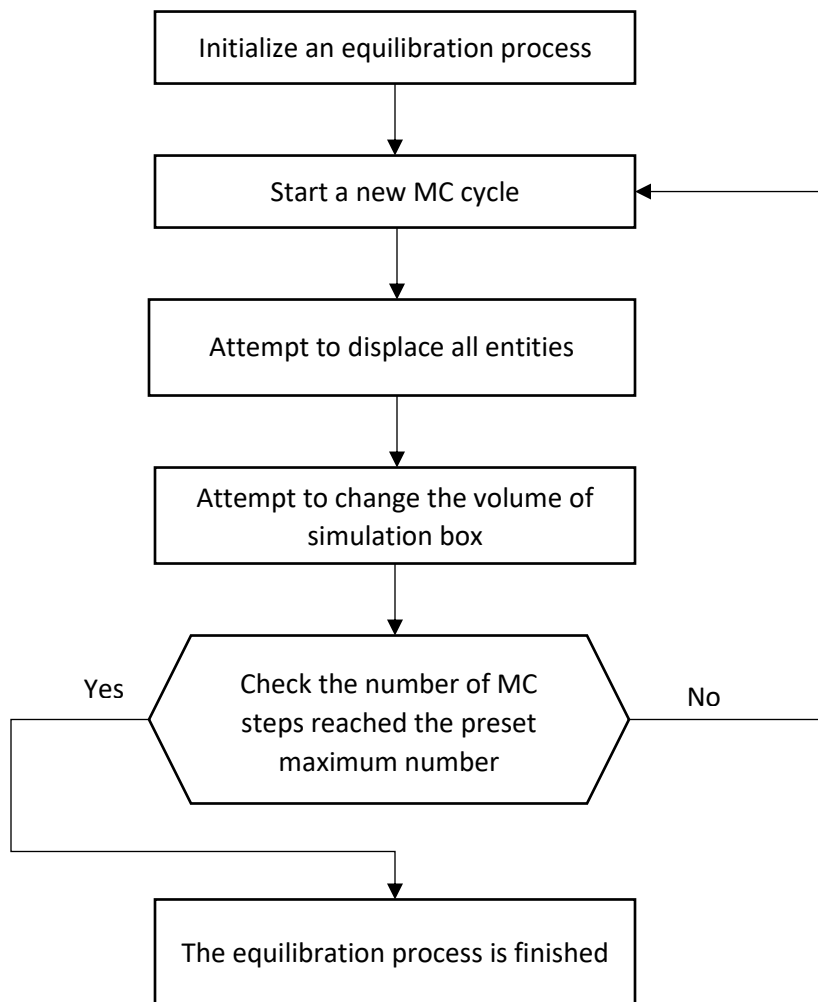


Figure 4.2 System equilibration flowchart.

4.3 Crosslinking Reactions

Cross-linking reactions are supposed to be the most important part of the simulation work, after this cross-linking reactions, system reaction conversion can be gained. A detailed procedure is listed below:

Step 1. Initialize the response simulation by setting the MC cycle index (I) and the crosslinking reaction conversion percentage (α_1) to 0.

Step 2. Start a new MC cycle by setting $I=I+1$, and let $T = T_i$ to update the system temperature.

Step 3. Attempt to displace a randomly selected entity by following the sub-steps below:

Step 3.1. Select randomly an entity that has not been selected in the current MC cycle. The position vector of the entity (namely entity i) is r_i .

Step 3.2. Calculate a new position for entity i, r_i^{trial}

Step 3.3. Reject the attempt and go to Step 4 if it violates the minimum distance restriction and the bond length restriction; otherwise, continue.

Step 3.4. Move the entity to the new position, if the attempt is accepted according to the Metropolis criterion; otherwise, this step attempt must be discarded.

Step 4. Perform crosslinking reactions between the selected entity and other entities by following the sub-steps below:

Step 4.1. Check if the selected entity i is a polymer bead or not.

Step 4.2. Check if there is a remaining functional group on this polymer bead or not. If yes, continue; otherwise, go to Step 5.

Step 4.3. Check if there is such a neighboring polymer bead j: (i) it has not been attempted to react with polymer bead i in the current run of Step 4, (ii) it is located within a reaction distance (l_{max}^r) from polymer bead i, (iii) it has a different type of functional groups, and (iv) it has at least one remaining functional group for reaction. If all these conditions are met, continue; otherwise, go to Step 5.

Step 4.4. Create a bond between polymer beads i and j with a specified probability. This

reaction probability, p^r is a function of system temperature T , i.e,

$$p^r = \min \left\{ 1, \eta \exp \left(\frac{-\Gamma^r}{k_B T} \right) \right\} \quad (4.3.1)$$

where η and Γ^r are material dependent parameters (both positive).

Step 4.5. Return to Step 4.2 for another possible bond creation.

Step 5. Check if all the entities have been attempted to displace once or not in the current MC cycle. If yes, continue; otherwise, return to Step 3.

Step 6. Calculate cross-linking conversion α_i using

$$\alpha_I = \alpha_{I-1} + \frac{N_{I-1}^A - N_I^A}{N_0^A} \quad (4.3.2)$$

where N_I^A is the number of remaining Type A functional groups in the end of the I -th MC cycle.

Thus, $N_{I-1}^A - N_I^A$ provides the number of bonds created in the I -th MC cycle.

Step 7. Check if $\alpha_I < \alpha_{max}$, where α_{max} is the target cross linking conversion. If yes, return to Step 2; otherwise, terminate the simulation as the network formation is accomplished.

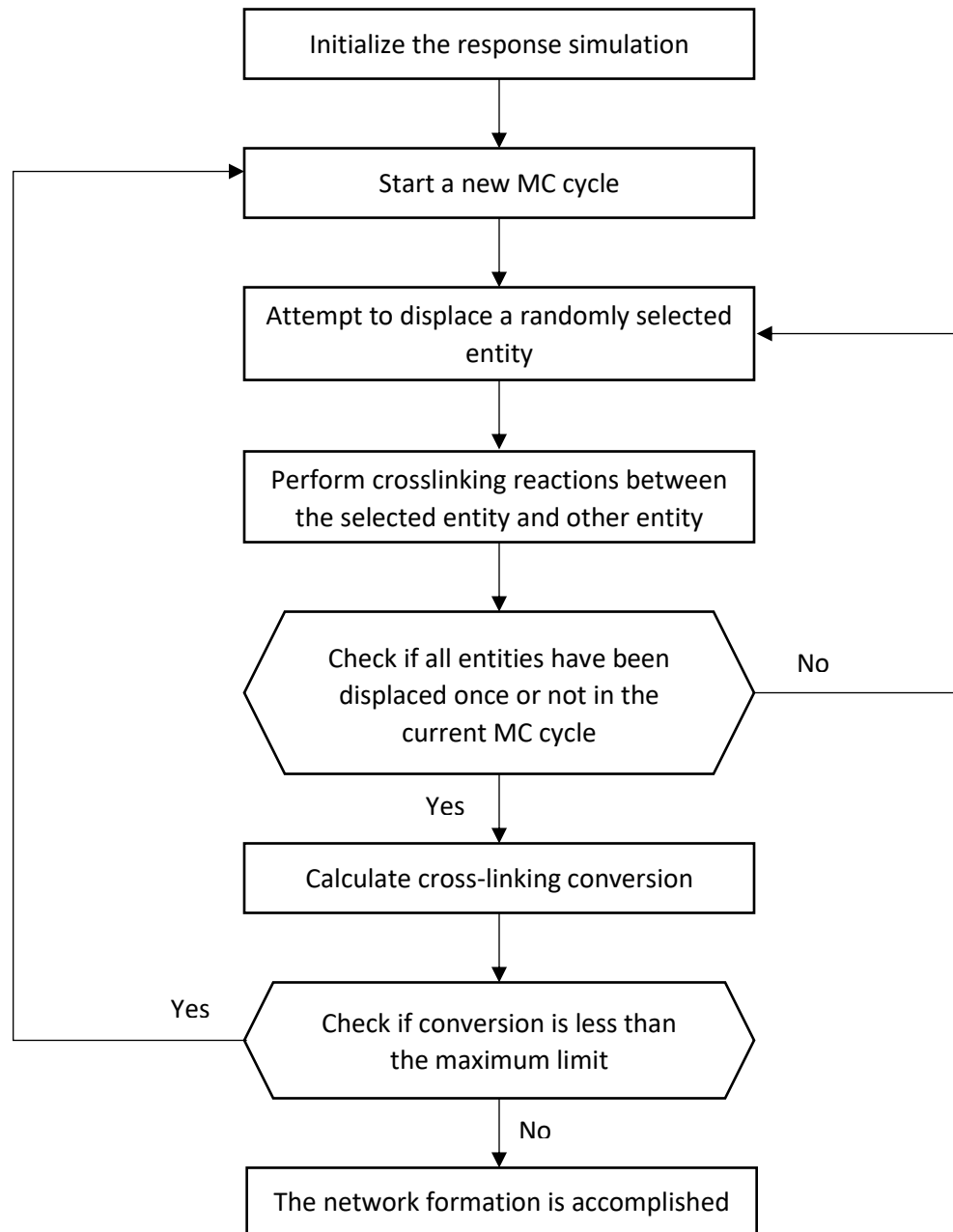


Figure 4.3 Cross-linking reaction flowchart.

4.4 Cooling Process

After the second equilibration, the system needs to be cooled to a normal temperature. The cooling procedure is conducted at a constant pressure. The cooling process can be achieved by following steps:

Step 1. Initialize the cooling process simulation by setting the MC cycle index (I) to 0, and then enter an initial temperature (T^h), an ending temperature (T^t), an external pressure (P^{ext}), and a desirable cooling rate (ΔT), and then let the system temperature T_I be T^h .

Step 2. Start a new MC cycle by setting $I=I+1$ and let $T_I = T_{I-1} + \Delta T$.

Step 3. Attempt to displace each entity by following Sub-steps 3.1 to 3.5 of the System Equilibration Procedure introduced previously.

Step 4. Attempt a volume change of the simulation box by following Sub-steps 4.1 to 4.4 of the System Equilibration Procedure introduced previously.

Step 5. Check if $T_I < T^t$ or not. If yes, the cooling process is ended; otherwise, return to Step 2.

After finish cooling procedure, the thermoset nano coating is at normal temperature. By computational calculation, all the numeral data can be recorded.

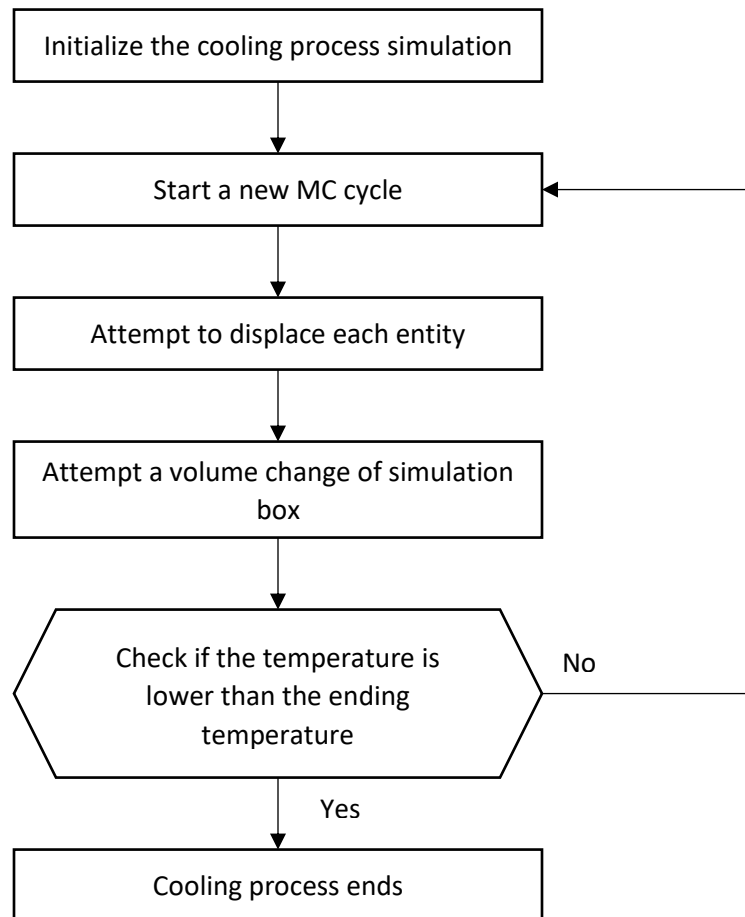


Figure 4.4 Cooling process flowchart.

4.5 Coating Testing and Quality Evaluation

After simulating the curing process, the quality of the coating is still needed to find a way out to present. Particularly for physical properties, it directly affects the product function. One of the most important physical parameters is Young's modulus. Young's modulus can determine the elastic property and the stiffness of coatings. Based on previous work, either within Monte Carlo simulation method or Molecular dynamics, Young's modulus can be quantified by a stress-strain

curve (Frankland et al., 2003; Cho and Sun, 2007; Adnan et al., 2007). Based on their work, some limitation of Young's modulus has been mentioned, such as a small system size and an unrealistic deformation rate. Since polymer system is not low and to keep the practicability of this methodology, Monte Carlo simulation is more suitable in this case. Series of off-lattice Monte Carlo are available for the deformation simulation of a single polymer chain, polymer melts and crosslinked polymer networks (Wittkop et al., 1994; Holzl et al., 1997; Chui and Boyce, 1999; Li et al., 2006).

The deformation of a thermoset coatings is not an equilibrium process. To make successful the deformation process, off-lattice Monte Carlo method will be used in this work. Based on the statement of Chui and Boyce (1999), Monte Carlo-based deformation can be regarded as an energy minimization procedure. In a high crosslinked polymer coating system, polymer chains are restricted, which means their movability is limited by the cross-linked network.

Strain Imposition: Like a general tensile test, stresses is applied to coating samples and by justifying the tensile strain, Young's modulus can be calculated. In this tensile test simulation part, by imposing a series of pressure increments ($\Delta\xi$) on the simulation box until the stain reaches its maximum value (ξ_{max}). The length increment at a preferred direction (e.g., the x direction) can be expressed as

$$\Delta l^x = l_I^x - l_{I-1}^x = l_0^x \Delta \xi, I = 1, 2, \dots, I_{max} \quad (4.5.1)$$

where l_I^x and l_{I-1}^x are respectively the box length at x direction after and before strain increment apply; I_{max} is the total number of strain increment and it also can be expressed as

$$l_{max} = \text{int}\left(\frac{\xi_{max}}{\Delta\xi}\right) \quad (4.5.2)$$

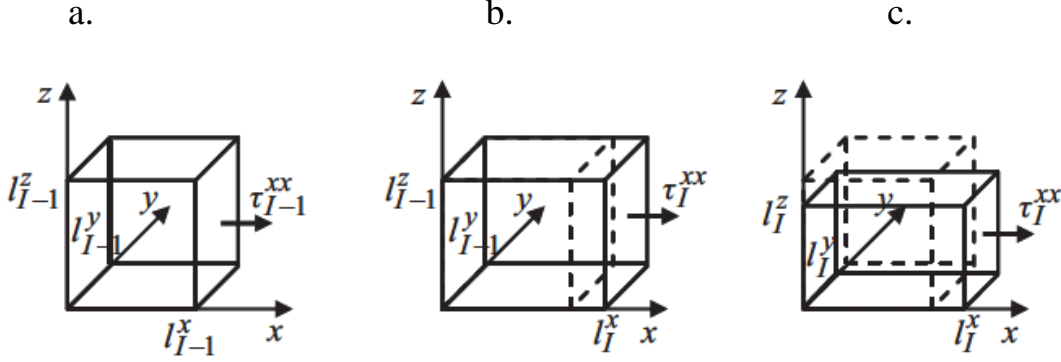


Figure 4.5.1 Sketch of a simulation box: (a) before imposing the i -th strain increment, (b) after imposing the i -th strain increment, (c) after the system relaxation (Xiao et al., 2009).

Figure 4.5.1 (a) and (b) present the simulation box length increment in x -direction before and after a strain apply. At this stage, the length in the other directions y and z are not changed. As the simulation box length changes, the entities in the simulation box will change accordingly. In the work of Chui and Boyce (2009), affine motion is introduced to predict the position of entity positions, which provides

$$r_{i,I} = \left(\left(\frac{l_I^x}{l_{I-1}^x} \right) x_{i,I-1}, y_{i,I-1}, z_{i,I-1} \right) \quad (4.5.3)$$

System Relaxation: In order to simulate a real material deformation process, a relaxation is required between two strain increments. To achieve a system relaxation, an ensemble containing the total number of entities (N^e) is fixed. That the stress in the transverse directions τ_x^{yy} and τ_x^{zz} are also fixed is assumed (Pickett et al., 2009).

In order to achieve a system relaxation in an extended ensemble which is named $N^e(l^x \tau_x^{yy} \tau_x^{zz})T$, the procedure which was introduced in the system equilibration section should be adopted. To adopt the equilibration section, the simulation box length should be replaced by the small size one and besides x direction, the pressure is in the pressure of atmospheric (P^{ext}) is closed to zero comparing the applied tensile stress. The adopted Step 4 is listed below.

Step 4. Change the size of the simulation box by following the sub-steps below:

Step 4.1. Check if $P^{dif} = \left| \frac{1}{2}(\tau_x^{yy} + \tau_x^{zz}) - P^{ext} \right|$ is lower than the maximum allowable deviation (P_{max}^{dif}) or not. If yes, go to Step 5; otherwise, continue.

Step 4.2. Attempt to change the box size by calculating the new box lengths in the y , and z directions, i.e.

$$l^{y,trial} = l^{y,now} + l_{max}^v(2\zeta - 1) \quad (4.5.4)$$

$$l^{z,trial} = l^{y,trial} \quad (4.5.5)$$

Step 4.3. The trial positions of all the entities become

$$r_i^{trial} = \left(x_i^{now}, \left(\frac{l^{y,trial}}{l^{y,now}} \right) y_i^{now}, \left(\frac{l^{z,trial}}{l^{z,now}} \right) z_i^{now} \right), i = 1, 2, \dots, N^e \quad (4.5.6)$$

Step 4.4. Reject the attempt and return to Step 4.2, if it violates either the minimum distance restriction or the bond length restriction; otherwise, continue.

Step 4.5. Move all the entities to the new positions, and return to Step 4.1 if $P^{dif,trial} < P^{dif,now}$; otherwise, return to Step 4.2.

Stress Evaluation: Normal stress needs to be evaluated in a unidirectional tensile test by the Virial theorem (Allen and Tildesley, 1987). Under the normal temperature, the kinetic stress can be neglected and provides

$$\tau^{\beta\beta} = \frac{1}{V_0} \sum_{i=1}^{N^e-1} \sum_{j=i+1}^{N^e} \left(\frac{d\Gamma_{i,j}}{dr} \Big|_{r_{i,j}} \frac{(r_{i,j}^\beta)^2}{r_{i,j}} \right), \beta\beta = xx, yy, \text{ or } zz \quad (4.5.7)$$

where $\tau^{\beta\beta}$ is the $\beta\beta$ component of the stress; V_0 is the volume of the simulation box before deformed; $r_{i,j}$ and $r_{i,j}^\beta$ are the norm and the β -component of the vector separating entities i and j respectively.

As in the nanoparticles applied system, two entities with different sizes should be considered, By replacing $r_{i,j}$ by $r_{i,j} - \omega_{i,j}R^n$ and $r_{i,j}^\beta$ by $r_{i,j}^\beta \left(1 - \frac{\omega_{i,j}R^n}{r_{i,j}}\right)$, the equation above can be evaluated, and the new equation provides

$$\tau^{\beta\beta} = \frac{1}{V_0} \sum_{i=1}^{N^e-1} \sum_{j=i+1}^{N^e} \left(\frac{d\Gamma_{i,j}}{dr} \Big|_{r_{i,j}} \left(\frac{r_{i,j}^\beta}{r_{i,j}} \right)^2 (r_{i,j} - \omega_{i,j}R^n) \right) \quad \beta\beta = xx, yy, \text{ or } zz \quad (4.5.8)$$

where $\omega_{i,j}$ is defined as

$$\omega_{i,j} = \begin{cases} 0, & i \text{ and } j \text{ are all polymer beads} \\ 1, & i \text{ and } j \text{ are one nano - particle and one polymer bead} \\ 2, & i \text{ and } j \text{ are all nano - particles} \end{cases}$$

There are four interactions between beads:

- I. The interaction between non-bonded polymers.
- II. The interaction between bonded polymers.
- III. The interaction between polymer and nanoparticle.

IV. The interaction between nanoparticles. Therefore, the equation above can be evaluated

as

$$\tau^{\beta\beta} = \tau^{\beta\beta,I} + \tau^{\beta\beta,II} + \tau^{\beta\beta,III} + \tau^{\beta\beta,IV} \quad \beta\beta = xx, yy, \text{ or } zz \quad (4.5.9)$$

Based on the Equations 3.3.1-3.3.4 where four types of potential energies are defined, and using Equation 4.5.9, the four types of stresses can be provided as

$$\tau^{\beta\beta,I} = \left(\frac{24\varepsilon^{pp}\sigma^6}{V_0} \right) \sum_{i=1}^{N^m+N^c-1} \sum_{\substack{j=i+1 \\ j \text{ and } i \text{ are bonded}}}^{N^m+N^c} \left(\frac{r_{i,j}^\beta}{r_{i,j}} \right)^2 \left(\left(\frac{1}{r_{i,j}} \right)^6 - 2\sigma^6 \left(\frac{1}{r_{i,j}} \right)^{12} \right) \quad (4.5.10)$$

$$\begin{aligned} \tau^{\beta\beta,II} = & \left(\frac{\mu(l_{max}^b)^2}{V_0} \right) \sum_{i=1}^{N^m+N^c-1} \sum_{\substack{j=i+1 \\ j \text{ and } i \text{ are bonded}}}^{N^m+N^c} \frac{(r_{i,j}^\beta)^2}{(l_{max}^b)^2 - (r_{i,j})^2} + \\ & \left(\frac{24\varepsilon^{pp}\sigma^6}{V_0} \right) \sum_{i=1}^{N^m+N^c-1} \sum_{\substack{j=i+1 \\ j \text{ and } i \text{ are bonded}}}^{N^m+N^c} \left(\frac{r_{i,j}^\beta}{r_{i,j}} \right)^2 \left(\left(\frac{1}{r_{i,j}} \right)^6 - 2\sigma^6 \left(\frac{1}{r_{i,j}} \right)^{12} \right) \end{aligned} \quad (4.5.11)$$

$$\tau^{\beta\beta,III} = \left(\frac{24\varepsilon^{pn}\sigma^6}{V_0} \right) \sum_{i=1}^{N^m+N^c} \sum_{j=N^m+N^c+1}^{N^e} \left(\frac{r_{i,j}^\beta}{r_{i,j}} \right)^2 \left(\left(\frac{1}{r_{i,j-R^n}} \right)^6 - 2\sigma^6 \left(\frac{1}{r_{i,j-R^n}} \right)^{12} \right) \quad (4.5.12)$$

$$\tau^{\beta\beta,IV} = \left(\frac{24\varepsilon^{nn}\sigma^6}{V_0} \right) \sum_{i=N^m+N^c+1}^{N^e-1} \sum_{j=i+1}^{N^e} \left(\frac{r_{i,j}^\beta}{r_{i,j}} \right)^2 \left(\left(\frac{1}{r_{i,j-2R^n}} \right)^6 - 2\sigma^6 \left(\frac{1}{r_{i,j-2R^n}} \right)^{12} \right) \quad (4.5.13)$$

Simulation Procedure: In order to have a more reliable prediction, three independent tensile tests in x, y, and z directions should be performed to obtain three stress-strain curves. The overall stress-strain behavior of a coating sample should be represented by an averaged stress-strain curve (Cho and Sun, 2007). The procedure is introduced below for conducting tensile tests on a coating sample.

Step 1. Specify the maximum strain (ξ_{max}), the strain increment ($\Delta\xi$), and the number of MC cycles (N_{max}^{MCC}) between two adjacent strain increments.

Step 2. Initialize a tensile test simulation in a coordinate direction β (i.e., x, y, or z) that has not been tested and set the strain increment index (I) and the initial strain (ξ_0) to 0. Then input the original simulation box size (l_0^x, l_0^y and l_0^z) and the undeformed coating microstructure, and successingly calculate the stresses, $\tau_0^{\beta\beta}$, $\tau_0^{\beta\beta,I}$, $\tau_0^{\beta\beta,II}$, $\tau_0^{\beta\beta,III}$ and $\tau_0^{\beta\beta,IV}$ using Equations 4.5.9-4.5.13.

Step 3. Update the strain increment index (let $I=I+1$), increase the strain by $\Delta\xi$, and increase the length of simulation box by Δl^β according to Equation 4.5.1

Step 4. Relax the system in the extended ensemble for N_{max}^{MCC} MC cycles.

Step 5. Evaluate stresses $\tau_I^{\beta\beta}$, $\tau_I^{\beta\beta,I}$, $\tau_I^{\beta\beta,II}$, $\tau_I^{\beta\beta,III}$ and $\tau_I^{\beta\beta,IV}$ using Equations 4.5.9-4.5.13.

Step 6. Check if $\xi_I < \xi_{max}$ or not. If yes, return to Step 3; otherwise, the tensile test in one coordinate direction is finished, and thus record all the strain and stress data.

Step 7. Check if all three coordinate directions have been tested or not. If no, return to Step 2; otherwise, output the strain and stress data in three directions and the coating sample testing is accomplished.

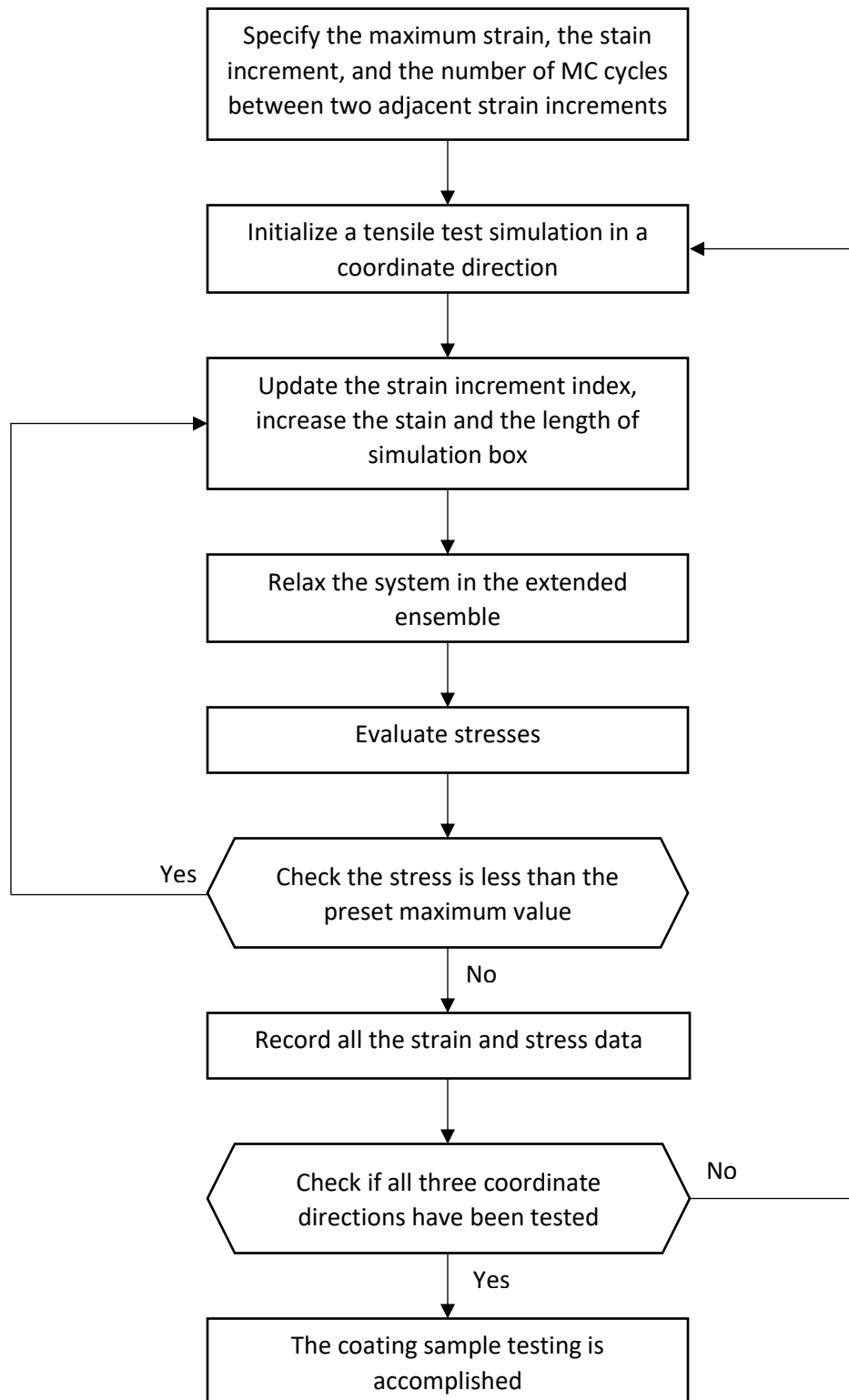


Figure 4.5 Coating testing simulation process flowchart.

Property and Quality Evaluation: Using the initial slope of the average stress-strain curve I the strain range up to ξ_{max}^Y (about 1%-2%). The quantification of E from the stress-strain data can be formulated as the following optimization problem

$$\min_E \sum_{I=0}^{I_{max}^Y} (E\xi_I - \bar{\tau}_I)^2 \quad (4.5.14)$$

where

$$\bar{\tau}_I = \frac{\tau_I^{xx} + \tau_I^{yy} + \tau_I^{zz}}{3} \quad (4.5.15)$$

$$I_{max}^Y = \text{int} \left(\frac{\xi_{max}^Y}{\Delta\xi} \right) \quad (4.5.16)$$

Note that I_{max}^Y is the number of strain increments imposed when the strain reaches ξ_{max}^Y .

On the other hand, various efforts have been devoted to correlating scratch resistance to a wide variety of material properties, such as crosslink density, network homogeneity, glass transition temperature, modulus, toughness, hardness, and coefficient of friction (Kutschera and Sander, 2006; Ryntz and Britz, 2002; Shen et al., 1997). Therefore, in this thesis, the scratch resistance is only correlated to the elastic modulus.

CHAPTER 5

CASE STUDY

To fully develop this methodology, a case study investigation is carried out for the curing process of nano coating. It is especially critical for studying the connections between curing conditions and cured coating properties. The result can also be suitable for curing process optimization or a prediction of assets change of nano coating. Several series of simulation tasks are designed and tested. From the simulation results, some analysis and explanation will be provided.

5.1 Material Specification

Polymer material: The thermoset material of interest is a resin with the polymer number average molecular weight of 3000 (Xiao et al., 2010). The assumed total number of monomers is 8660, which is adjusted by our previous work. Other material parameters are listed below:

Table 5.1 Parameter settings for TSNCs model and simulation.

Parameters	Values
$r_{max}^{pp^*}$	2.50
$r_{min}^{pp^*}$	0.79
$r_{max}^{pn^*} - R^{n^*}$	4.49

$r_{min}^{pn^*} - R^{n^*}$	0.85
$r_{max}^{nn^*} - 2R^{n^*}$	4.49
$r_{min}^{nn^*} - 2R^{n^*}$	0.85
μ	30.00
$l_{max}^{b^*}$	1.5
$l_{min}^{bf^*}$	1.02
$l_0^{b^*}$	0.97
$l_{max}^{r^*}$	1.20
η	1×10^{10}
Γ^{r^*}	27.7
ξ_{max}^Y	0.02

5.2 Base Case Analysis

In the baseline scenario (case 1), as a reference group, polymer coatings are assumed to be cured in general curing process which is under elevated temperature starting from 300k ending with 400k. To find out the relationship between real curing time and simulation MC steps, the maximum conversion is set as 80% which is regarded as a value of curing completion conversion. The final amount of MC steps can roughly present 30 mins in the curing process.

In case 2, 5% nano SiO_2 is simulated to be applied in coatings' curing process. By investigating, the value reached at 80% conversion, the effect of nano particles can be seen. If simulation works well, a post-curing phenomenon can be clearly read through the data. However, to predict the time which reaching a higher conversion takes, the maximum conversion is set as 90%.

In case 3, the conversion change after nano coating curing process is investigated. The proposal of this instance is to predict how the conversion will change when nanocoating finishes curing at a room temperature after the conversion reaches a significant value which is 70. In case 4, a curing process only under room temperature is investigated. Considering some devices would not satisfy a curing oven, curing only under room temperature is included in this work. Since curing under room temperature is typically regarded as a slow process, a maximum number of MC steps are set instead of maximum conversion.

Table 5.2 Parameter set up for all cases.

Case Number	NP Percentage	Max MC Steps	Max Conv.	T(K)
1	0%	Unlimited	80%	300-400
2	5%	Unlimited	90%	300-400
3	5%	300k	Unlimited	300-400-300
4	5%	300k	Unlimited	300

5.3 Simulation Results

All cases have been simulated 6 times, and the average values are taken in this section. Since Monte Carlo simulation has its randomness characteristic, data from each test may have a small difference. Figure 5.3.1 shows the conversion change of the curing process without nano components. Totally, it takes 2860 MC steps to reach a conversion of 80%. Before arriving at a significant conversion value (around 10%), the curing process conducts very slowly. This is because when first polymer beads try to build bonds, some of the distance between two beads would not satisfy the constraint conditions so that the attempt of building bond fails. Another reason is that at the beginning of the curing process, the temperature of the coating process is still low. With the temperature raising, it is easier to have polymer beads bonded. However, after reached another significant conversion value (around 68%); the crosslinking process tends to slow down. This is because the number of left available unbounded beads is getting smaller. The limited number of polymer beads restricts the occurrence of the bond establishment. Between these two values, cross-linking process conducts relatively steady and fast.

Therefore, the entire curing process can be generalized to three stages. In stage 1, as there are a lot of molecules near a function group, the chance to form a covalent bond is feeble. From the view of collision theory, for each function group, it takes more time to impact a satisfied molecule. In simulation language, a significant amount of MC steps is spent on verifying restrictions between two random particles. In stage 2, as stage 1 has helped to filtrate part of satisfied molecules, the curing speed is faster than that in stage 1, because the amount of verifying

time reduces and the correct collision happens more frequently. In stage 3, the number of unverified molecules reduces, collision reaction becomes more difficult than the collision in stage 2. The curing speed slows down again. The unbounded molecules can hardly satisfy the restrictions. Coating extends to fully cured state.

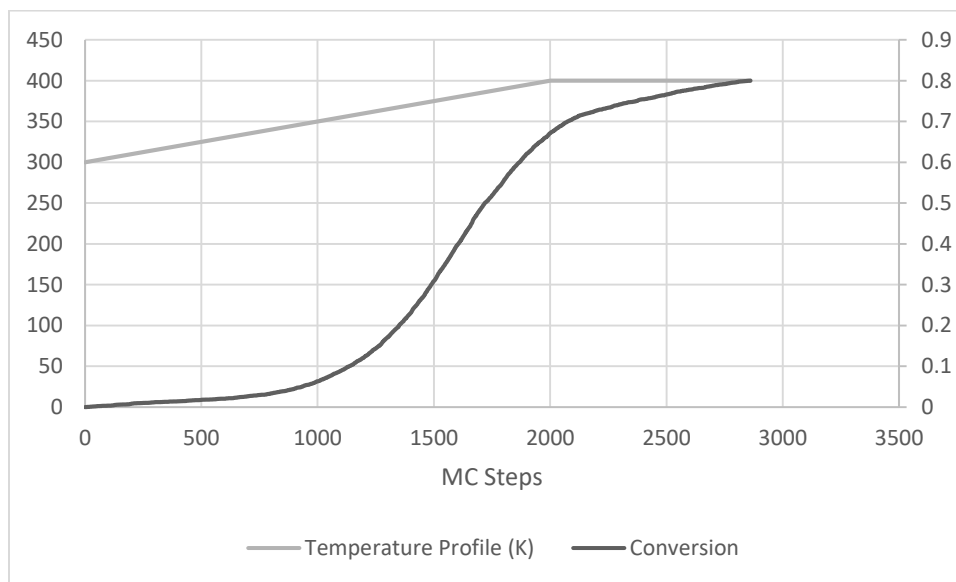


Figure 5.3.1 Pure polymer coating curing process.

Figure 5.3.2 shows the conversion change in a curing process with 5% nano-silica applied. With the application of nano-silica, the whole curing process is delayed. From the numerical data, because of the application of nano-silica, conversion reaches 80% at a step of 3320. 16% more MC steps are spent after nano-silica is applied. In other words, if the curing temperature and time are fixed, the conversion of nano coating is lower than the transformation of clear polymer coating when they get out of curing oven. This can be used to explain the phenomenon in figure 2.1.3. About the shape of the whole curing process, an explanation is provided above. The line hits 0.9

at the stop of 8400, which means it will take about 2.53 times steps to increase another 10% conversion from 80%.

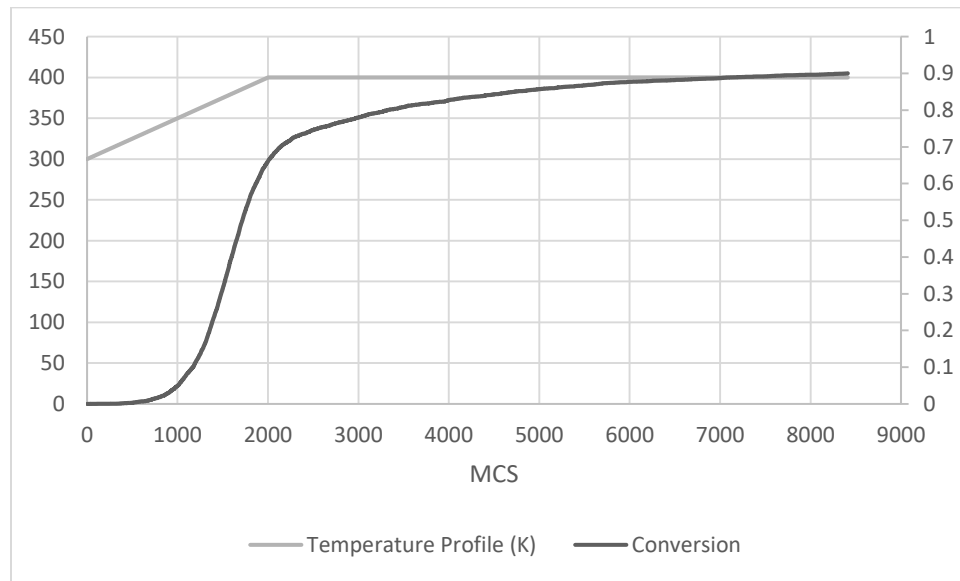


Figure 5.3.2 Nano coating curing process with 5% SiO₂ applied.

Figure 5.3.3 shows the conversion change in case 3. Comparing Figure 5.3.2 and Figure 5.3.3, the natural curing process is even much slower than it which is under oven temperature. From the numerical data, conversion hits 70% at the steps of 2050, but after 30k steps, the conversion is 70.46%. The curing process does happen at room temperature, but it is extremely slower than that under oven temperature. However, Monte Carlo steps can not exactly express the real curing time. The number of MC steps dramatically increase to finish a try of building a bond between beads because the left available unbounded beads are rare. In other words, even with the same difference value of MC steps, the real curing time may multiply increase.

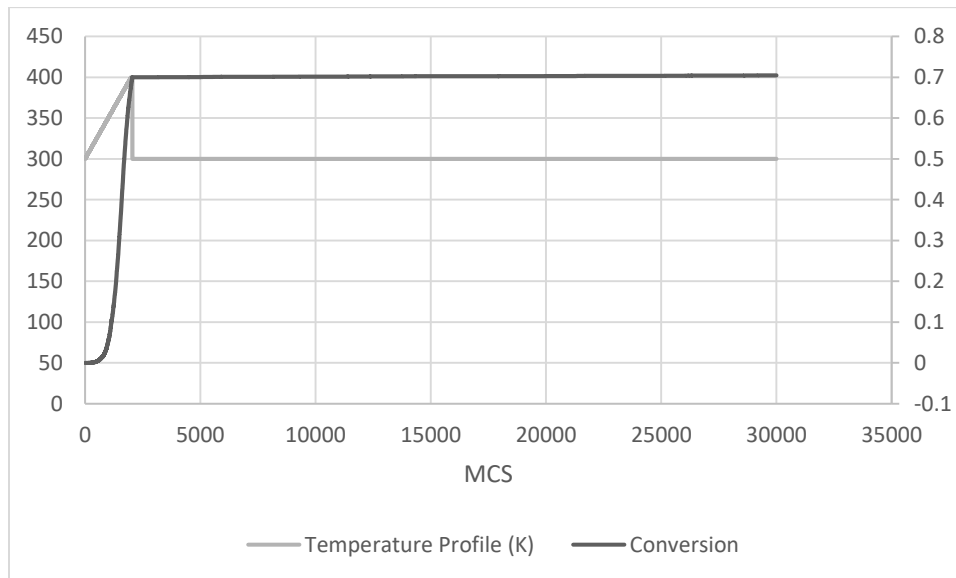


Figure 5.3.3 Nano coating curing process before and after reach 70%.

Figure 5.3.4 shows the curing process under 300k room temperature. Under the chamber temperature, the natural curing process also occurs. After 30k MC steps, conversion reaches 62.44%. Comparing Figure 5.3.3 and Figure 5.3.4, curing speed under room temperature is much slower in higher conversion. In lower conversion, it takes 300k steps to reach 62.44%, but after hitting 70%, it takes roughly 2.8k steps to make a change of 0.46%. Collision theory can explain this phenomenon. Temperature is one of the most important factors that affects the collision energy which further influences the curing process. But note that, the curing temperature is not the higher, the better. The temperature should be considered by different category of curing agent and also should be determined by Differential Thermal Analysis (DTA).

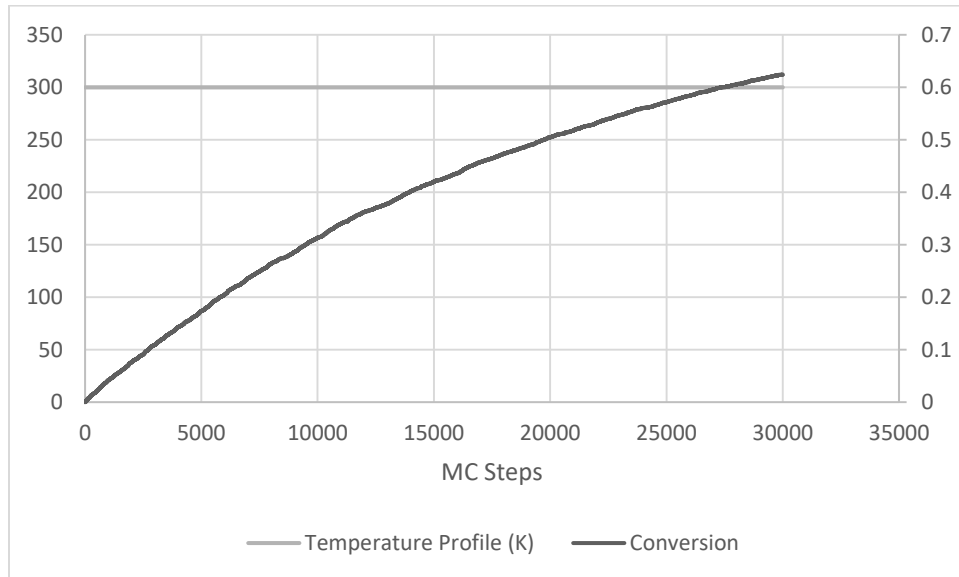


Figure 5.3.4 Nano coating curing process only under room temperature.

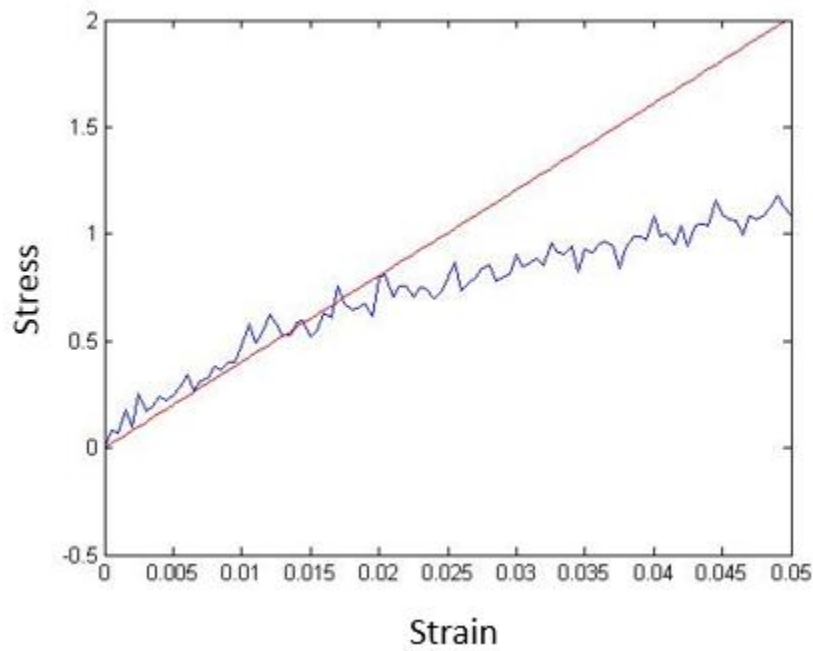


Figure 5.3.5 An example of stress and strain curve which is achieved by using steps in 4.5.

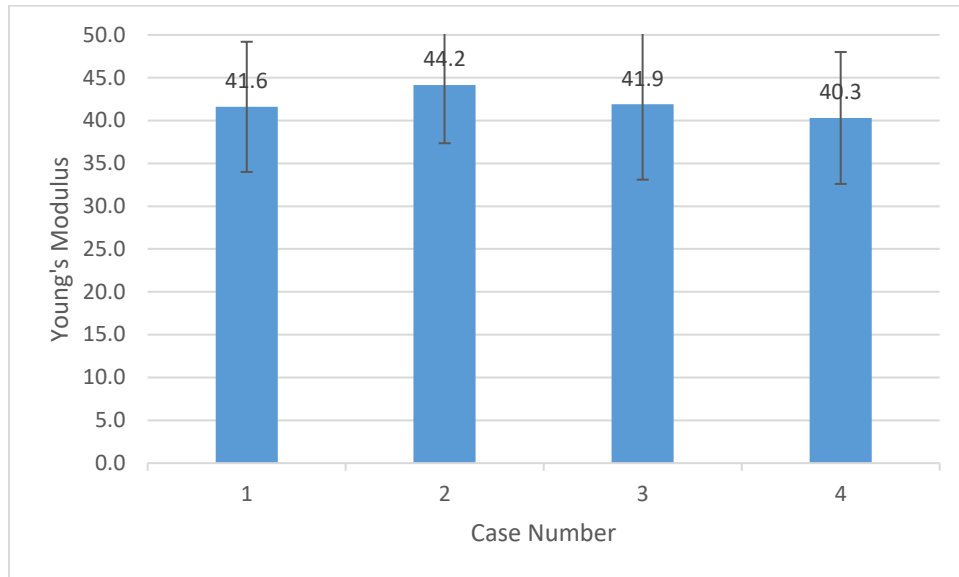


Figure 5.3.6 Final Young's Modulus value in each case.

Figure 5.3.5 shows an example of using steps in 4.5 to calculate Young's Modulus. The initial slope of stress to strain represents the Young's Modulus based on Hooke's law.

Figure 5.3.6 shows the final Young's Modulus values from each case. The overall trend is that with the same material, a higher conversion leads a better Young's Modulus value. Generally, higher Young's Modulus expresses better physical properties, such as scratch resistance. On the other hand, Young's Modulus values in case 1, and 3 are very close which can also show that nano-silica improves the physical properties. 5% nano-silica presents 10% conversion benefits.

5.4 Summary

In this chapter, all cases are simulated by programming, and results show that post-curing works an important role in quality control. The thorough understanding of curing and post-curing

can significantly help with product and procedure design. All simulation results have perfectly matched the collision theory. The conversion change in a curing process is S-shape. A Huge amount of particles in early stage reduces the possibility of actual collision, and after highly cured effective collision happens infrequently. Both reasons will lead a slow curing process. The curing speed between two stages is relatively faster than the speed in the early and post-curing process. A conclusion can be drawn that in the same curing procedure, nanoparticles resist the progress of cross-linking, which presents as a lower conversion and mechanical strength when curing process ends.

On the other hand, at the same conversion, nano-silica provides a significant improvement in physical properties. In other words, even though applying nano-silica reduces the physical properties when products come out of manufacturing, properties still get enhanced after the long-term post-curing process. Because of the existence of the post-curing phenomenon, it is possible to redesign production process and the plan of energy usage. The specific curing process still needs to be determined by manufacturing objectives and production demand.

CHAPTER 6

CONCLUSION

6.1 Conclusions

Thermoset nanocomposites are the polymer composite materials that can dramatically improve appealing properties and offer new functionalities in the resulting coating. With filling different nanoparticles, coatings will gain fantastic functional change to satisfy the various demand. In the automotive coating industry, nanocoating has gained attention for its capability of offering superior physical properties. Adding nano silica can enhance the scratch resistance of coatings. Furthermore, people are looking forwards to achieving more functional improvement by applying nanocomposites such as nano TiO₂ and nano ZnO. On the other hand, when nanocomposites give new functional enhancement, they also bring challenges in manufacturing and product quality control, especially in the curing operation. With the same curing process, the conversion of polymer components cannot reach the same value as any nanocomposites accretion. During the polymer matrix network formation, nanoparticles reduce the volume of the share so that nanocoatings need more time to convert polymer beads to network structure at the same temperature. The post curing phenomenon is discovered after vehicles exposed to the environment. The conversion slowly increases at normal temperature and part of physical functions even increase. This leads a problem of how to explain the phenomenon and it is even challenging in product quality control.

In this thesis, plenty research on nanocomposites has been reviewed and analyzed. The effects of nanocomposites from different types, sizes, heterogeneities and shapes are listed and analyzed. A conclusion can be drawn that nanocomposites sensitively affect certain physical properties such as scratch resistance, thermal and optical stability. A deep understanding of how nanocomposites work together with polymer beads is necessary for further study of nano technique and nano products. Computational product design through Monte Carlo simulation should be an effective way for nanocoating development study. Also, some other computational work has been reviewed to satisfy the simulation demand in different service stage. By using Monte Carlo simulation method, a series of dynamic curves have been gotten. The conversion change can be clearly seen in the simulation results and different cases have been set up for a deep understanding. The results explain how nanocomposites interact with polymer components and how fast conversion changes in both curing and post curing stages.

Another contribution of this thesis is to provide a methodology to make a prediction for saving energy. Sustainability is always the hot topic for industries, especially for energy saving. Because of the existence of post curing phenomenon, which is effected by nano components, industries may need to redesign the curing process and conditions for achieving the best properties with lowest energy use. On the other hand, for special usage coatings which are designed to be cured at normal temperature, this work can provide an efficient method to estimate the duration of curing period.

6.2 Future Work

From what has been reviewed and simulated, some of the characters haven't been considered in this work, for example, heterogeneity and shape. To achieve a more comprehensive analysis and prediction, further work on characterizing more parameters is necessary. Also, all technique references which are used in this work are all research based. Experiment data is needed to revise the veracity of these results. Conceivably, this kind of approach is not sufficient for an accurate prediction. As mentioned above, the real time for each MC step varies as the conversion changes. The generation of the contrast between real time and MC steps is necessary.

Since Monte Carlo simulation method has its random characteristic which is considered as a match for polymer network formulation, there may show different results between each computational work. Extensive tests is needed to filtrate ridiculous result, which takes more time to achieve more reliable simulation data. Additional work can also be done to improve the computational efficiency by adjusting code writing.

REFERENCES

- Allen, N. S., M. Edge, A. Ortega, C. M., Liauw, J. Stratton, and R. B. McIntyre, "Behaviour of nanoparticle (ultrafine) titanium dioxide pigments and stabilisers on the photooxidative stability of water based acrylic and isocyanate based acrylic coatings," *Polymer Degradation and Stability*, **78**(3), 467-478 (2002).
- Allen, N. S., M. Edge, A. Ortega, C. M. Liauw, J. Stratton, and R. B. McIntyre, "Degradation and stabilisation of polymers and coatings: nano versus pigmentary titania particles," *Polymer degradation and stability*, **85**(3), 927-946 (2004).
- Allen, M.P., D.J. Tildesley, "Computer Simulation of Liquids," *Clarendon Press*, Oxford (1987)
- Ahmadi, B., M. Kassiriha, K. Khodabakhshi, and E. R. Mafi, "Effect of nano layered silicates on automotive polyurethane refinish clear coat," *Progress in Organic Coatings*, **60**(2), 99-104 (2007).
- Cho, J., C.T. Sun, "A molecular dynamics simulation study of inclusion size effect on polymeric nanocomposites," *Computational Material Science*, **41**, 54-64 (2007).
- Dhoke, S. K., A. S. Khanna, and T. J. M. Sinha, "Effect of nano-ZnO particles on the corrosion behavior of alkyd-based waterborne coatings," *Progress in Organic Coatings*, **64**(4), 371-382 (2009).
- Doh, S. J., C. Kim, S. G. Lee, S. J. Lee, and H. Kim, "Development of photocatalytic TiO₂ nanofibers by electrospinning and its application to degradation of dye pollutants," *Journal of hazardous materials*, **154**(1), 118-127 (2008).

- Fufa, S. M., B. P. Jelle, P. J. Hovde, and P. M. Rørvik, "Coated wooden claddings and the influence of nanoparticles on the weathering performance," *Progress in organic coatings*, **75**(1), 72-78 (2012).
- Fufa, S. M., B. P. Jelle, and P. J. Hovde, "Weathering performance of spruce coated with water based acrylic paint modified with TiO₂ and clay nanoparticles," *Progress in Organic Coatings*, **76**(11), 1543-1548 (2013).
- Gu, X., D. Zhe, M. Zhao, G. Chen, S. S. Watson, P. E. Stutzman, and J. W. Martin, "More durable or more vulnerable?—Effect of nanoparticles on long-term performance of polymeric nanocomposites during UV exposure," *International Journal of Sustainable Materials and Structural Systems*, **1**(1), 68-94 (2012).
- Jalili, M. M., and S. Moradian, "Deterministic performance parameters for an automotive polyurethane clearcoat loaded with hydrophilic or hydrophobic nano-silica," *Progress in Organic Coatings*, **66**(4), 359-366 (2009).
- Kiil, S. "Model-based analysis of photoinitiated coating degradation under artificial exposure conditions," *Journal of Coatings Technology and Research*, **9**(4), 375-398 (2012).
- Kiil, S. "Mathematical modeling of photoinitiated coating degradation: Effects of coating glass transition temperature and light stabilizers," *Progress in Organic Coatings*, **76**(12), 1730-1737 (2013).
- Kremer, K., G.S. Grest, "Dynamics of entangled linear polymer melts: a molecular dynamics simulation" *Journal of Chemistry and Physics*, **92**(1), 5057-5086 (1990).
- Kutschera, M., R. Sander, "Scratch resistance of automobile clearcoat: chemistry and characterization on the micro-and nanoscale," *JCT Research*, **3**, 91-97 (2006).

- Metropolis, N., A.W. Rosenbluth, M.N. Teller, and E. Teller, "Equation of state calculations by fast computing," *Journal of Chemistry and Physics*, **21**(4), 1087-1092 (1987).
- Mirabedini, S. M., M. Sabzi, J. Zohuriaan-Mehr, M. Atai, and M. Behzadnasab, "Weathering performance of the polyurethane nanocomposite coatings containing silane treated TiO₂ nanoparticles," *Applied Surface Science*, **257**(9), 4196-4203 (2011).
- Ortelli, S., M. Blosi, C. Delpivo, D. Gardini, M. Dondi, I. Gualandi, and S. A. Tofail, "Multiple approaches to test nano TiO₂ photo-activity," *Journal of Photochemistry and Photobiology A: Chemistry*, **292**, 26-33 (2014).
- Pang, Y., S. S. Watson, and L. P. Sung, "Surface degradation process affected by heterogeneity in nano-titanium dioxide filled acrylic urethane coatings under accelerated UV exposure," *Polymer*, **55**(25), 6594-6603 (2014).
- Pickett, J. E., J. R. Sargent, H. A. Blaydes, and N. Babbie, "Effects of temperature on the weathering lifetime of coated polycarbonate," *Polymer Degradation and Stability*, **94**(7), 1085-1091 (2009).
- Rajagopalan, N., and A. S. Khanna, "Effect of size and morphology on UV-blocking property of nanoZnO in epoxy coating," *International Journal of Scientific and Research Publications*, **3**, 1-14 (2013).
- Ryntz, R.A., D. Britz, "Scratch resistance behavior of automotive plastic coatings," *JCT Research*, **74**, 77-81 (2002).
- Skaja, A., D. Fernando, and S. Croll, "Mechanical property changes and degradation during accelerated weathering of polyester-urethane coatings," *JCT research*, **3**(1), 41-51, (2006).

- Vacatello, M., "Monte Carlo simulations of polymer melts filled with solid nanoparticles," *Macromolecules*, **34**, 1946-1952 (2001).
- Vacatello, M., "Molecular arrangements in polymer-based nanocomposites," *Macromolecules Theory Simulation*, **44**, 757-765 (2002).
- Xiao J. and Y. Huang, "Microstructure-property-quality-correlated paint design: a lattice Monte Carlo based approach," *AIChE J.*, **55**(1), 132-149 (2009).
- Xiao, J., Y. Huang, and C. Manke, "Computational design of thermoset nanocomposite coatings: Methodological study on coating development and testing," *Chemical Engineering Science*, **65**(2), 753-771 (2010).
- Yang, X. F., C. Vang, D. E. Tallman, G. P. Bierwagen, S. G. Croll, and S. Rohlik, "Weathering degradation of a polyurethane coating," *Polymer degradation and stability*, **74**(2), 341-351 (2001).
- Yari, H., S. Moradian, and N. Tahmasebi, "The weathering performance of acrylic melamine automotive clearcoats containing hydrophobic nanosilica," *Journal of Coatings Technology and Research*, **11**(3), 351-360 (2014).
- Yari, H., S. Moradian, N. Tahmasebi, and M. Arefmanesh, "The effect of weathering on tribological properties of an acrylic melamine automotive nanocomposite," *Tribology Letters*, **46**(2), 123-130 (2012).

ABSTRACT**MONTE CARLO SIMULATION BASED
PRODUCT QUALITY ANALYSIS OF
POLYMER COATING CURING AND POST CURING**

By

Jianming Zhao**May 2017****Advisor:** Dr. Yinlun Huang**Major:** Chemical Engineering**Degree:** Master of Science

To achieve better property of polymer coatings, different categories of nanoparticles are applied before coating's curing process. However, one of the adverse effects is the change of final property, which leads the difficulty of product quality control. Using mathematical modeling method can actually improve the cost and time to get a prediction of product quality. Still now, different series of models are developed for various purposes. For example, Monte-Carlo simulation suits short-term usage prediction; kinetics simulation suits long-term usage prediction; potential energy simulation suits to model microcosmic particle's energy change.

To solve the difficulty of quality control, Monte-Carlo simulation is used to provide relatively accurate data under given conditions. A series of models are redesigned, based on those developed by Xiao et al. (2009, 2010). From the simulation data, a visualized conversion and final Young's modulus change can be clearly seen.

In this thesis, a linear plot of the general curing process is gained. Monte Carlo simulation methodology is a new method to describe the conversion change. The post-curing process is also simulated, with the contrast of the real data from Yari (2014), the post-curing process and principle can be explained. The effect of the nanoparticle can also be gained in this work. Additionally, with the work of this thesis, people can control the product quality more easily.

AUTOBIOGRAPHICAL STATEMENT

JIANMING ZHAO

EDUCATION

- **M.S., Chemical Engineering and Material Science, Wayne State University**
- **B.S., Polymer Material and Science, Dalian University of Technology, 2013**

AWARDS

- **Graduate Tuition Scholarship, Wayne State University, 2014**
- **Scientific and Technological Inventions Scholarship, Dalian University of Technology, 2009**

PROFESSIONAL EXPERIENCE

- Conducted Monte-Carlo Simulation to predict the property change under different curing conditions in the curing and post-curing process of polymer coatings
- Developed a series of model to analyze the photo-initiated degradation of epoxy-amine applied by nano-SiO₂ under artificial exposure conditions for long-term usage
- Designed and operated the experiment to toughen multifunctional epoxy resin with PPENK to achieve more pressure and heat resisting material